

THE CRYSTAL CHEMISTRY OF STAUROLITE. I. CRYSTAL STRUCTURE AND SITE POPULATIONS

FRANK C. HAWTHORNE*, LUCIANO UNGARETTI, ROBERTA OBERTI, FRANCA CAUCIA
AND ATHOS CALLEGARI

CNR Centro di Studio per la Cristallografia e la Cristallografia, via Bassi 4, I-27100 Pavia, Italy

ABSTRACT

The crystal structures of 42 samples of staurolite have been refined to *R* indices of 1–2% using single-crystal MoK α X-ray data. Samples were selected to cover as wide a range of compositions as possible, and site populations were assigned by site-scattering refinement and *via* the development of mean bond-length – cation-radius relationships for the staurolite structure. The cation site-nomenclature is revised to give a scheme that is more convenient and compatible with schemes of site nomenclature in other rock-forming silicate minerals. The chemical composition that best approximates most examples of staurolite is Fe_{3.4}[T(2),M(4)] Al₂ □₂[M(3)] Al₁₆[M(1),M(2)] Si₈[T(1)] O₄₈ H_{2.4} with the occupancies indicated. Staurolite is monoclinic, [C2/m, observed β between 90 and 90.45°], the β angle correlating with the differential occupancy and sizes of the M(3A) and M(3B) octahedra. Positional disorder was observed at the T(2) site, which is occupied by Fe, Zn, Li, Co, Mg, Al and □ (vacancy); there is some indication that the disorder in T(2) correlates with variation in the β angle. Site-scattering refinement shows small but significant occupancy of M(1) [= M(1A) + M(1B)], M(2) and M(3) [= M(3A) + M(3B)] by transition-metal cations. Detailed consideration of chemical compositions and mean bond-lengths shows significant Mg occupancy of M(1), M(2) and M(3). In most staurolite samples, ~40% of the Mg occupies the octahedrally coordinated M(1), M(2) and M(3) sites; the remainder occupies the tetrahedrally coordinated T(2) site. There is a considerable range of M(4) scattering (0.0–11.5 electrons pfu); several arguments show M(4) to be occupied by Fe (+ □), except for one very Mg-rich sample of staurolite (Mg \approx 3 apfu), in which M(4) is occupied by Mg. There is also significant variation in the refined scattering at the M(3) site, spanning the range 1.75–2.09 cations (Al) pfu. Both the high occupancy of M(4) and the low occupancy of M(3) are correlated with increased H content. Local order involving cations and vacancy at the T(2) and M(4) sites is a very important feature of the staurolite structure; stereochemical arguments allow quantitative assignment of vacancies to the T(2) site from the refined M(4) site-scattering.

Keywords: staurolite, crystal-structure refinement, electron-microprobe analysis, ion-microprobe analysis, site populations, order–disorder.

SOMMAIRE

La structure cristalline de monocristaux de staurolite provenant de quarante-deux échantillons a été affinée jusqu'à un résidu *R* de 1 à 2% en utilisant des données obtenues avec rayonnement MoK α . Les échantillons ont été choisis pour couvrir, dans la mesure du possible, la gamme complète de compositions de cette espèce. L'occupation des sites a été déterminée par affinement du pouvoir de dispersion à chaque site, et par la relation nouvelle entre longueur de liaison moyenne dans cette structure et rayon cationique. Nous proposons une révision de la nomenclature de chaque site, pour la rendre plus commode et compatible avec le protocole de nomenclature d'autres silicates pétrologiquement importants. La formule chimique qui répond le mieux à la composition de la plupart des échantillons serait Fe_{3.4}[T(2),M(4)] Al₂ □₂[M(3)] Al₁₆[M(1),M(2)] Si₈[T(1)] O₄₈ H_{2.4}, avec l'occupation des sites telle qu'indiquée. La staurolite est monoclinique, C2/m, β observé entre 90 et 90.45°, l'angle β montrant une corrélation avec l'occupation et la dimension différentielles des sites octaédriques M(3A) et M(3B). Nous mettons en évidence un désordre de position au site T(2), qu'occupent Fe, Zn, Li, Co, Mg, Al et □ (lacune); ce désordre pourrait avoir un lien avec la variation dans l'angle β . L'affinement du pouvoir de dispersion montre une occupation faible mais importante des sites M(1) [= M(1A) + M(1B)], M(2) et M(3) [= M(3A) + M(3B)] par des ions des métaux de transition. Une considération détaillée des compositions chimiques et des longueurs de liaison moyennes démontre un niveau important de Mg dans les sites M(1), M(2) et M(3). Dans la plupart des échantillons, environ 40% du Mg occupe les sites à coordination octaédrique M(1), M(2) et M(3). Le reste se trouve dans le site T(2), à coordination tétraédrique. Il y a une variation considérable dans la dispersion associée au site M(4) (entre 0 et 11.5 électrons par unité formulaire); nous proposons, plusieurs arguments à l'appui, que M(4) contient Fe (+ □), sauf dans un cas de staurolite fortement magnésienne (environ 3 atomes de Mg par unité formulaire), où c'est le Mg qui occupe M(4). Nous trouvons aussi une grande variation dans la dispersion associée au site M(3), équivalente à une variation entre 1.75 et 2.09 cations (Al) par unité formulaire. Le taux élevé d'occupation de M(4) et le faible

*Permanent address: Department of Geological Sciences, University of Manitoba, Winnipeg, Manitoba R3T 2N2.

taux d'occupation de $M(3)$ sont associés avec une teneur élevée en hydrogène. Une mise en ordre locale impliquant cations et lacunes aux sites $T(2)$ et $M(4)$ serait un aspect très important de la structure de la staurolite; des arguments d'ordre stéréochimique permettent une attribution quantitative des lacunes au site $T(2)$ à partir de l'affinement de la dispersion associée au site $M(4)$.

(Traduit par la Rédaction)

Mots-clés: staurolite, affinement de la structure cristalline, analyse à la microsonde électronique, analyse à la microsonde ionique, occupation des sites, ordre-désordre.

INTRODUCTION

Staurolite is a common mineral in metapelitic rocks, and is diagnostic of medium-grade metamorphism. Its widespread occurrence and sensitivity to conditions of equilibration suggest that it should be a good indicator of metamorphic conditions. However, problems associated with most aspects of its crystallography, crystal chemistry and phase equilibria have prevented its effective use in petrogenetic work, and conflicting results from experimental (Pigage & Greenwood 1982) and field studies (*e.g.*, Holdaway *et al.* 1988) are common.

Staurolite is monoclinic with $\beta \approx 90^\circ$, and is also

pseudo-orthorhombic. Its composition is not particularly complicated, but recent confirmation that both H (Lonker 1983, Holdaway *et al.* 1986a) and Li (Dutrow *et al.* 1986, Holdaway *et al.* 1986b) are significantly variable components shows that earlier efforts to understand the chemistry of staurolite were hindered by incomplete information. The principal difficulty arises in trying to decipher the site populations. This involves assigning Al and Mg, and Fe^{2+} and Fe^{3+} (+ minor Ti, Cr, Zn, with sometimes major Zn, Co and now Li) to several crystallographically distinct sites in the structure, including sites that are pseudosymmetrically related by the pseudo-orthorhombic symmetry. Although this is in principle no more difficult than in

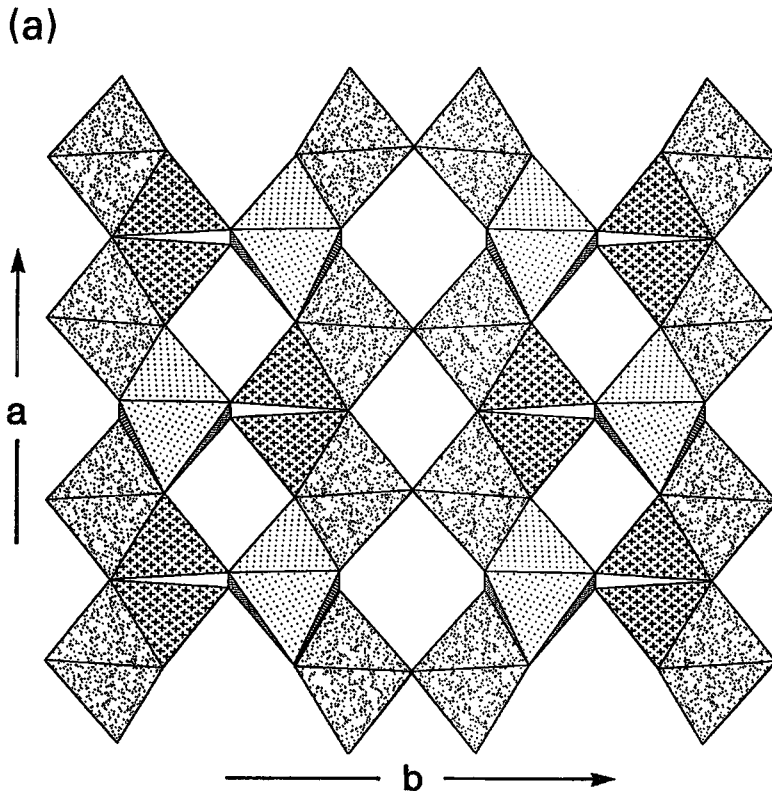
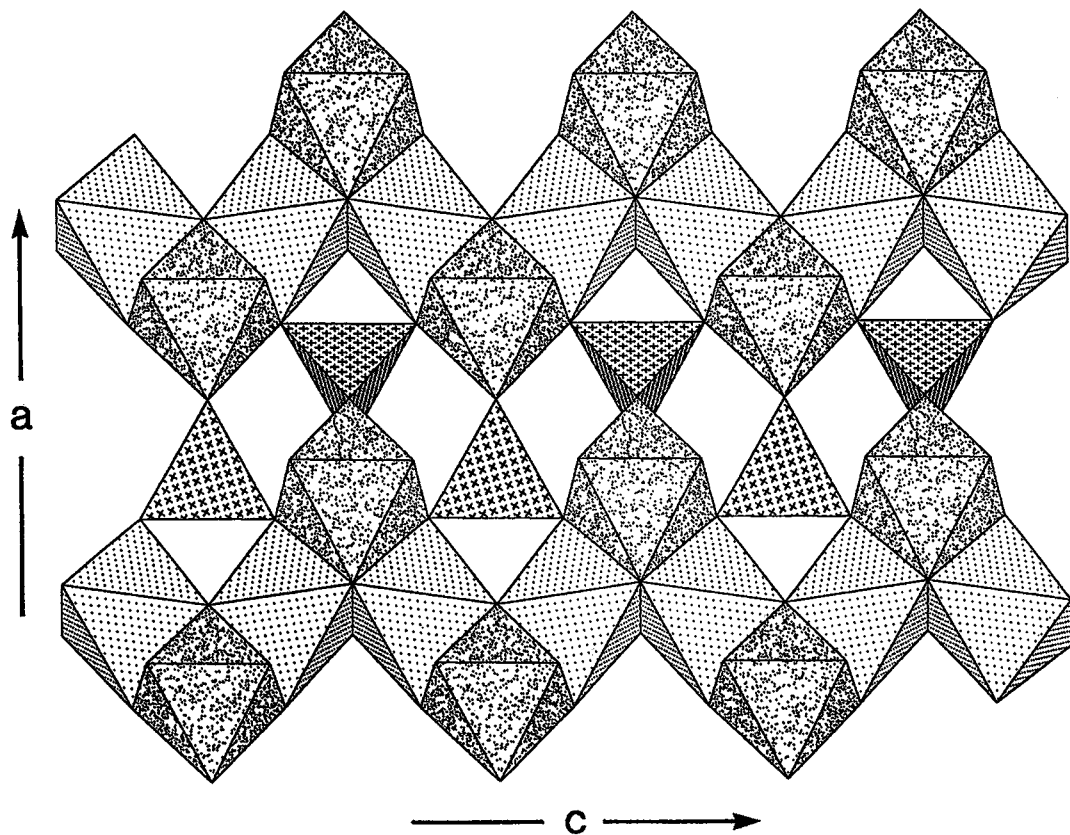
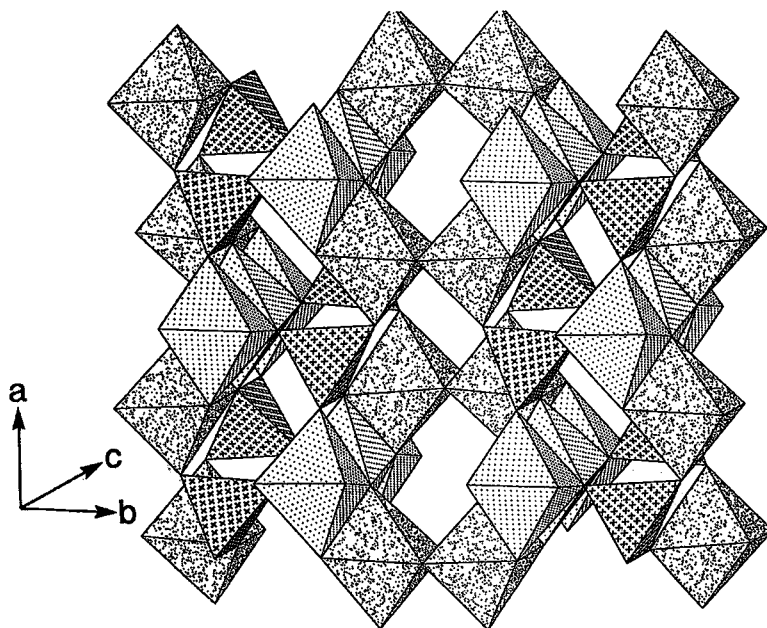


FIG. 1. The crystal structure of staurolite, showing the kyanite-like part of the structure. The $M(1A)$ and $M(1B)$ octahedra are regularly dot-shaded; the $M(2)$ octahedron is irregularly dot-shaded, and the $T(1)$ tetrahedron is shaded with crosses; (a) the structure viewed down [001]; (b) the structure viewed 15° away (in the (001) plane) from [010]; note the serrated octahedral edge-sharing chains that are cross-linked by $T(1)$ tetrahedra; (c) an oblique view of the structure, showing the interpolyhedral linkage.

(b)



(c)



the case of other complex rock-forming silicates (*e.g.*, amphiboles, pyroxenes), the problem is exacerbated by the fact that staurolite, unlike most other common ferromagnesian silicates, does not show wide (absolute) ranges of chemical composition. Consequently, the response of the structure to compositional variations is very subtle, and it is difficult to convincingly derive site populations by the usual methods of X-ray or neutron scattering and absorption spectroscopy.

The lack of accurate information on site populations means that it is impossible to derive thermodynamic data on adequately characterized material. In addition, it is also not feasible to develop reliable activity models for thermodynamic treatment. Significant progress has recently been made in the chemical characterization of staurolite (Dutrow *et al.* 1986, Holdaway *et al.* 1986a, b, Lonker 1983), making the question of site populations more pressing than ever. Here we attack this problem by crystal-structure refinement of a large number of staurolite samples covering the full compositional range of the natural minerals. A preliminary account of this work was given by Ungaretti *et al.* (1987).

SITE NOMENCLATURE

The site nomenclature currently used for staurolite is not satisfactory. Sites are identified by element symbols, a situation that is not very convenient where substitution of various types of cation occurs at the same site. The situation becomes absurd when the "Fe site" contains no Fe whatsoever, but Zn or Co instead. Consequently, we have relabeled the sites in staurolite according to the scheme shown in Table 1.

Tetrahedrally coordinated cations are labeled by the letter *T*, and octahedrally coordinated cations are labeled by the letter *M*. Anion sites retain the old labels, as these are compatible with the new scheme of labeling of the cations. The hydrogen positions are labeled H, but the subsequent letter designation differs from previous studies; these have been changed such that O(1A) is the donor oxygen for H(1A) and H(2A), and O(1B) is the donor oxygen for H(1B) and H(2B). The *A* and *B* designations for atoms have been

retained, as it is often convenient to consider pairs of atoms, bonds or sites together, and these can then be jointly labeled by the atom number alone [*e.g.*, *M*(1)]. There is an additional site, *T*(3), not found in previous studies; this occurs in oxidized staurolite (Caucia *et al.* 1994), and has been preliminarily described by Ungaretti *et al.* (1988); it is included here for completeness.

REVIEW AND SYNTHESIS OF PREVIOUS WORK

There has been much significant work done in the past few years, and a detailed review and synthesis of the current situation are warranted, both to highlight the principal problems in the crystal chemistry of staurolite, and to identify those factors that are currently the subject of controversy.

General structure

The structure of staurolite was essentially determined by Náray-Szabó (1929), using the orthorhombic space-group *Ccmm* and a chemical formula ($Z = 1$) $\text{Fe}_4\text{Al}_{16}\text{Si}_8\text{O}_{48}\text{H}_8$. In their description of lusakite, the cobalt analogue of staurolite, Skerl & Bannister (1934) noted both the difference between the formula used by Náray-Szabó (1929) and the previous formula proposed by Horner (1915), and also the similarity of the latter to the formula unit of lusakite: $[\text{Co}_{1.93}\text{Fe}^{2+}_{0.81}\text{Mg}_{1.09}\text{Ni}_{0.20}\text{Ti}_{0.11}]_{\Sigma 4.03}[\text{Al}_{16.76}\text{Fe}^{3+}_{1.06}]_{\Sigma 17.82}[\text{Si}_{7.75}\text{Al}_{0.25}]_{\Sigma 8}\text{O}_{48}\text{H}_{2.26}$. A careful morphological and X-ray study (Hurst *et al.* 1956, recounted in detail by Donnay & Donnay 1983) confirmed the *C*-centered lattice for staurolite, but also showed that staurolite is monoclinic with space-group symmetry *C2/m* (assuming the presence of a center of symmetry, as suggested by a negative piezoelectric test). At the same time, Juurinen (1956) reported what are now regarded (Holdaway *et al.* 1986b) as results of very high quality chemical analyses of staurolite, and gave a new idealized formula: $\text{Fe}_4\text{Al}_{18}\text{Si}_8\text{O}_{48}\text{H}_4$ (note that this has a net positive charge of 2+). These new data prompted a re-investigation of the staurolite structure by Náray-Szabó & Sasvári (1958), using the space group *C2/m* and the formula unit $\text{Fe}_4\text{Al}_{18}\text{Si}_8\text{O}_{48}\text{H}_2$. They showed that the original structural arrangement of Náray-Szabó (1929) was essentially correct, but that the *Ccmm* symmetry was only a pseudo-symmetry, and that the correct symmetry is *C2/m* with $\beta \approx 90^\circ$, later confirmed in detail by Smith (1968).

The staurolite structure (Fig. 1) is traditionally described as slabs of kyanite $[\text{Al}_2\text{SiO}_5]$ and Fe–Al-oxide-hydroxide $[\sim [{}^6\text{Al}_{0.7}{}^{42}\text{Fe}_2\text{O}_2(\text{OH})_2]$ alternating along [010]. As noted by Náray-Szabó (1929), this can also be described as a close-packed array of anions with ${}^6\text{Al}$, ${}^{42}\text{Fe}$ and ${}^{42}\text{Si}$ occupying the interstices. The kyanite layer is ideally $[\text{Al}_{16}\text{Si}_8\text{O}_{40}]$, but extensive

TABLE 1. REVISED NOMENCLATURE FOR CATION SITES IN STAUROLITE

New	Mult.	Old	New	Mult.	Old
M(1A)	4	Al(1A)	T(1)	8	Si
M(1B)	4	Al(1B)	T(2)	4	Fe
M(2)	8	Al(2)	T(3)	4	---
M(3A)	2	Al(3A)	H(1A)	4	P(1A), H(1B)
M(3B)	2	Al(3B)	H(1B)	4	P(1B), H(1A)
M(4A)	2	U(1)	H(2A)	4	H(2B)
M(4B)	2	U(2)	H(2B)	4	H(2A)

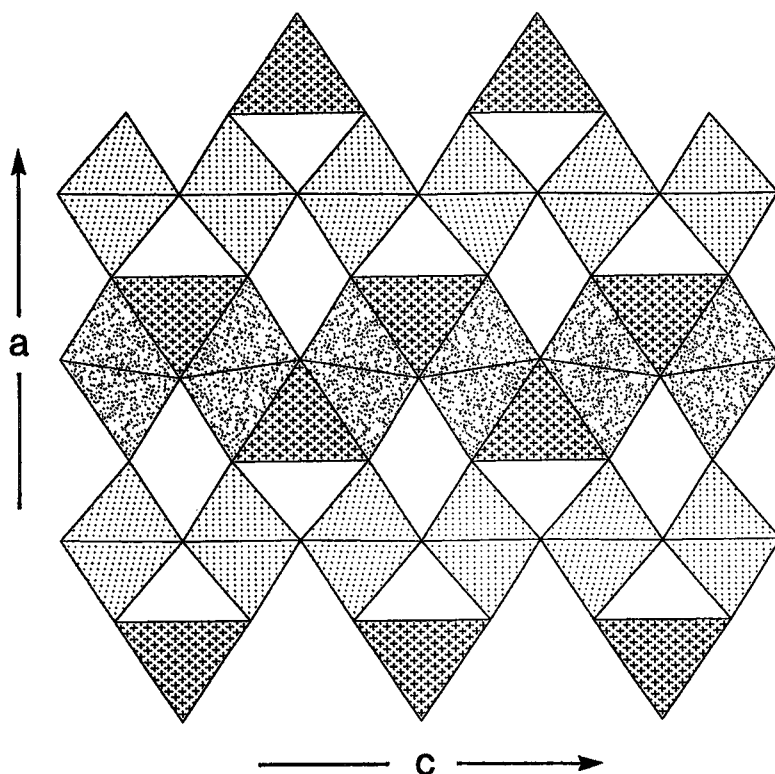


FIG. 2. Polyhedral representation of the oxide-hydroxide layer in staurolite. The $M(3A)$ and $M(3B)$ octahedra are regularly dot-shaded, the $M(4A)$ and $M(4B)$ octahedra are irregularly dot-shaded, and the $T(2)$ tetrahedron is shaded with crosses. Octahedra adjacent along $[001]$ share edges, and $T(2)$ tetrahedra share faces with $M(4A)$ and $M(4B)$ octahedra.

chemical data show significant $Al \rightleftharpoons Si$ and possibly $Fe \rightleftharpoons Al$ substitutions; however, the stereochemical details of these substitutions are not known. The oxide-hydroxide layer is far more complicated; this layer is illustrated in Figure 2. A (rutile-like) chain of edge-sharing octahedra extends along $[001]$. This chain is flanked by (FeO_4) tetrahedra, sharing vertices with adjacent octahedra and assuming a staggered arrangement on either side of the chain; the resulting $[M(TO_4)O_2]$ structural unit is a common one in many chemical classes of minerals (Hawthorne 1990). It has generally been assumed that the principal substitutions in the structure occur in the oxide-hydroxide layer; although small amounts of "cross-substitution" have been proposed by various investigators, crystal-chemical details are currently lacking.

Compositional range of staurolite

For such a complex mineral, staurolite has a sur-

prisingly small range of composition. More recent formulations have been variations of the type



in which the cation associations within parentheses do not necessarily restrict their substitution to the site(s) implied by the groupings.

First we will summarize the observed compositional ranges irrespective of the sites occupied by the particular cation. It should be noted here that antipathetic behavior of cation pairs (*e.g.*, Fe^{2+} , Mg) should not be taken as inferring direct 1:1 substitution at a specific site, as some authors have proposed more complex coupled substitutions involving cations of different valence at more than one type of site. Griffen & Ribbe (1973), Ribbe (1982) and Griffen *et al.* (1982) have considered the formula and observed compositional range of staurolite, assuming 4 H apfu (atoms per formula unit). The observed ranges (in apfu) are listed below:

Si	7.18–8.09	(7.09: Grew & Sandiford 1984)
Al	16.56–19.24	(19.91: von Knorring et al. 1979)
Fe	1.86–3.66	(0.16: Chopin, pers.comm.)
Mg	0–1.44	(3.01: Chopin, pers.comm.)
Zn	0–1.54	(2.13: Chopin, pers.comm.)
Ti	0–0.17	(0.34: Schreyer et al. 1984)
Mn	0–0.15	

Some of these ranges have been extended by more recent studies (values given in parentheses), and additional components have been recorded in significant amounts:

Cr	0–0.45	(Ward 1984a)
Co	0–1.94	(Skerl & Bannister 1934)
Ni	0–0.20	(Skerl & Bannister 1934)
Li	0–1.57	(Holdaway & Goodge 1990)

For at least some of these cations, it seems that the constraints on their range are geochemical rather than structural, as synthetic Mg (Schreyer & Seifert 1969), Zn (Griffen 1981) and Co (Phillips & Griffen 1986) end-members have been synthesized, albeit at high pressures.

Obviously, the compositional ranges given above are not independent, as overall electroneutrality must be maintained, and there may be further additional constraints due to local crystal-chemical factors such as bond-valence requirements or steric restrictions. A strong correlation (Fig. 3a) between $[Al - (8 - Si)]$ and $[Fe + Mg + Zn]$ was observed by Griffen *et al.* (1982), leading them to write a more general formula as $(Fe,Mg,Zn)_{25.6-1.25x}Al_{1.5x-8.2}Si_{16.2-0.5x}O_{48}H_4$, where $16.58 \leq x \leq 18.61$. This does not incorporate the examples of Co-rich staurolite that have been reported (Skerl & Bannister 1934, Čech *et al.* 1981, Bringhurst & Griffen 1986); renormalization of these compositions on the same basis as that used by Griffen *et al.* (1982) shows them to correspond to the trend of (Fe,Mg,Zn) -bearing staurolite shown in Figure 3a.

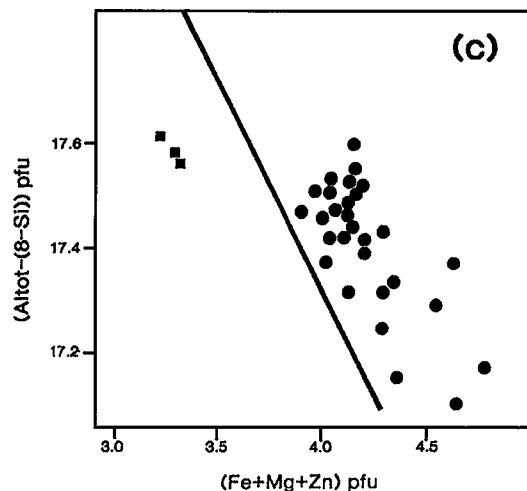
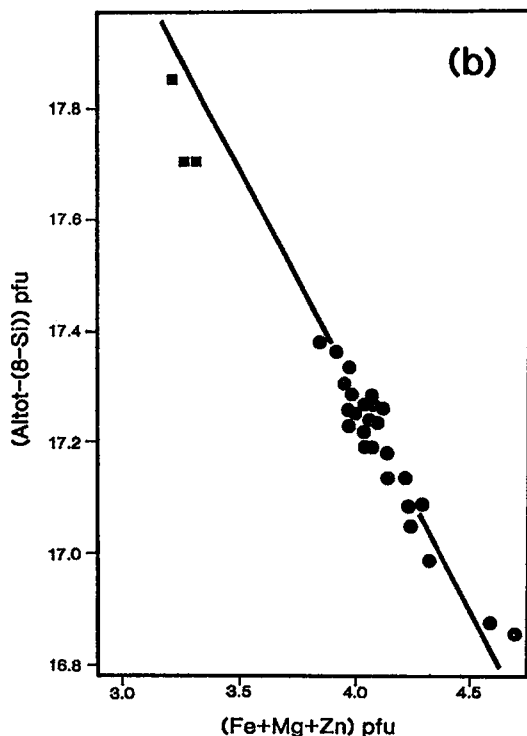
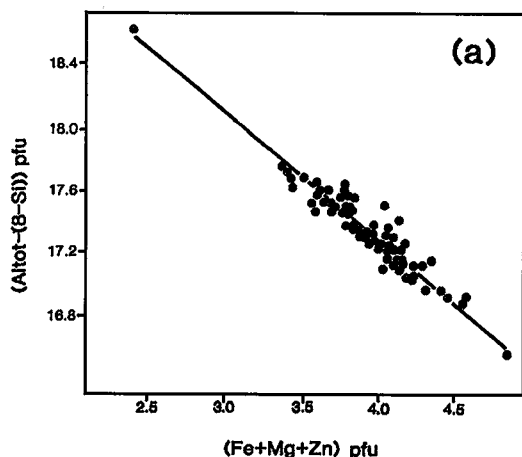


FIG. 3. Variation in $[Al - (8 - Si)]$ with $[Fe + Mg + Mn]$ in staurolite: (a) compilation of literature values normalized on the basis of $44 O^{2-} + 4 OH^-$, from Griffen & Ribbe (1973); (b) the staurolite compositions of Holdaway *et al.* (1986b) normalized on the basis of $44 O^{2-} + 4 OH^-$ and excluding Li_2O ; (c) the staurolite compositions of Holdaway *et al.* (1986b) normalized on the basis of $48 (O^{2-}, OH^-, F^-)$ and including Li_2O ; the line in (c) is the same as in (b). In (b) and (c), circles represent staurolite samples with $H \approx 3$ apfu; squares represent staurolite samples with $H \approx 4$ apfu.

However, the basis for the calculation of the formula unit used by Griffen *et al.* (1982) is now known to be inappropriate. They calculated their cell contents on the basis of 46 atoms of oxygen [= 44 O + 4 OH], assuming a constant H content of 4 apfu. Lonker (1983) and Holdaway *et al.* (1986a) have shown that H is a variable component in staurolite, with a range of 2.6–4.2 apfu. In addition, Dutrow *et al.* (1986) have shown that Li can be a significant component in some samples of staurolite. The effects of ignoring these two factors (variability of H, the presence of Li) are shown in Figures 3b and 3c, which show the data of Holdaway *et al.* (1986b) plotted in the same fashion, recalculated on the bases of [44 O + 4 OH] and 48 (O, OH, F), respectively. It is immediately obvious from Figure 3 that the correlation observed between $[Al]^{tot} - (8 - Si)$ and $[Fe + Mg + Mn]$ is induced primarily by the incorrect procedure for the unit-formula renormalization.

Thus the formula given above is based on the incorrect assumption that $H \approx 4$ apfu. In addition, the work of Dutrow *et al.* (1986) and Holdaway *et al.* (1986b) shows that the presence of Li is an important factor in some parageneses. Holdaway *et al.* (1986b) showed that the substituent species in staurolite fall into two well-defined groups:

- (i) $(R^{2+} + Li + 1/2 H)$ range: 5.69–6.28 $\sigma = 0.15$
 (ii) $(Si + Al)$ range: 25.10–25.61 $\sigma = 0.13$

in which the cation sums indicated show a very restricted range. Neither Li nor $(H + Li)$ show any correlation with Al, but $(R^{2+} + Li)$ shows a good correlation with $(H + F)$, with a slope of approximately 0.57 (Fig. 4a). This correlation suggests that the most important substitution involving hydrogen is



[not $2 H \rightleftharpoons (R^{2+} + Li)$ as written in Holdaway *et al.* (1986b)]. Note that (1) is charge-balanced, whereas the latter is not; Li must be included in the plot of Figure 4a, as it also affects the R^{2+} content *via* the substitution



(Dutrow *et al.* 1986), as illustrated in Figures 4b and 4c. It is notable that these "hidden substitutions" involving first-row elements (H, Li, Be, B) and vacancies have been a principal factor in inhibiting our understanding of the chemistry of some of the more complex common silicate minerals (*cf.*, Groat & Hawthorne 1989, Groat *et al.* 1989, 1992, Hawthorne *et al.* 1993).

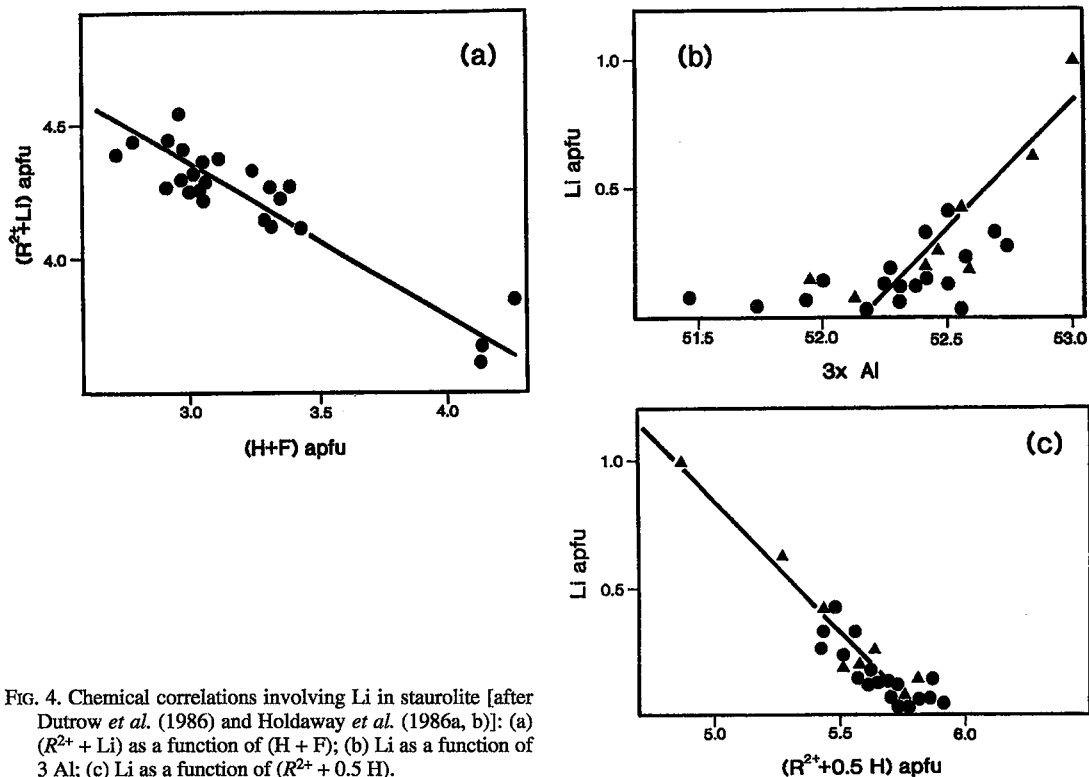


FIG. 4. Chemical correlations involving Li in staurolite [after Dutrow *et al.* (1986) and Holdaway *et al.* (1986a, b)]: (a) $(R^{2+} + Li)$ as a function of $(H + F)$; (b) Li as a function of $3 Al$; (c) Li as a function of $(R^{2+} + 0.5 H)$.

Hydrogen in staurolite

As is apparent from the previous discussions, the proposed H-content of staurolite has been very variable, from 2 apfu (Horner 1915) to 8 apfu (Náray-Szabó 1929). Results of most chemical analyses suggest that the H content is variable between 2 and 4 apfu (Takéuchi *et al.* 1972), but as noted by Holdaway *et al.* (1986a), the concentration of H is particularly difficult to determine in staurolite because of the mineral's refractory nature, the almost ubiquitous presence of inclusions, and the probable evolution of H in different forms (H_2O , H_2 , CH_4) on heating. Charge-balance calculations on unit-cell contents (*i.e.*, normalized on the basis of measured density) suggest a mean value of 4 H apfu (Griffen & Ribbe 1973), but this is obviously not a reliable method of renormalization for individual mineral formulae, given the difficulty of measuring an accurate density. A significant step toward the resolution of this problem was taken by Lonker (1983) and Holdaway *et al.* (1986a), both of whom reported careful determinations of H in staurolite samples from a variety of different localities. Both studies show that H varies significantly in staurolite, but they differ somewhat in the ranges observed. The data of Lonker (1983), measured on a modified Dupont moisture analyzer, vary from 1.8 to 3.6 apfu (0.95–1.92 wt% H_2O); the data of Holdaway *et al.* (1986a), measured on a H-isotope extraction-line and an ion microprobe, vary from 2.7 to 4.2 apfu (1.4–2.3 wt% H_2O). Holdaway *et al.* (1986a) concluded that the former data are systematically low by -0.3 – 0.6 wt% H_2O . Holdaway *et al.* (1986a) also noted that staurolite samples fall into two groups: (i) staurolite coexisting with garnet or biotite (or both) contain 2.7–3.4 H apfu (*i.e.*, a mean value of 3.06 H apfu); (ii) staurolite that does not coexist with either garnet or biotite contains 4.09–4.16 H apfu (*i.e.*, a mean value of 4.14 H apfu).

On the basis of local charge-balance (bond-valence) requirements, Hanisch (1966) proposed that the H atoms are attached to the O(1A) and O(1B) anions; this arrangement was confirmed by the two-dimensional refinement of a staurolite crystal by Takéuchi *et al.* (1972) using neutron-diffraction data. More accurate positions of the protons were subsequently provided by the three-dimensional neutron-diffraction refinement of the structure by Tagai & Joswig (1985); the O–H distances, 1.08(1) and 0.97(1) Å observed for O(1A)–H(1A) and O(1B)–H(1B), are each typical for an (OH) group (with significant hydrogen-bond interaction). However, site-scattering refinement showed neither hydrogen position to be completely occupied. The observed H occupancies of 0.38(1) and 0.48(2), respectively, for H(1A) and H(1B) indicate a cell content of 3.44 H apfu, within the range of 2.7–3.4 H apfu observed by Holdaway *et al.* (1986a) for staurolite coexisting with biotite. However, Ståhl *et al.* (1988)

have recently identified two additional hydrogen positions in a neutron-diffraction refinement of the structure of a staurolite crystal from Pizzo Forno, St. Gotthard, Switzerland. All hydrogen positions are shown diagrammatically in Figure 5. They all are ~ 1 Å away from the O(1A) and O(1B) oxygen atoms, as expected for hydroxyl groups. The positions H(1A) and H(2A) are ~ 1 Å apart, too close for simultaneous occupancy; H(1B) and H(2B) are likewise arranged, also too close for simultaneous occupancy [which would result in an (H_2O) group]. The position H(1A) is ~ 2 Å from both H(1B) and H(2B), a short distance for simultaneous occupancy of H(1A) and either H(1B) or H(2B); the local arrangement around H(1B) is similar. All of the H positions are less than half-occupied. Occupancy of specific H positions exerts constraints on the occupancies of adjacent sites, as discussed in detail by Ståhl *et al.* (1988). The latter also noted that the occurrence of the H(2A) and H(2B) sites in staurolite is concordant with the third proton nuclear magnetic resonance reported by Takéuchi *et al.* (1972).

Disorder of tetrahedrally coordinated cations in the oxide-hydroxide layer

In his refinement of the St. Gotthard staurolite, Smith (1968) found that within the oxide-hydroxide layer, tetrahedrally coordinated Fe^{2+} [at the T(2) site] shows significant positional disorder. For a structure model with a single T(2) position, difference-Fourier maps showed three maxima of residual density in the

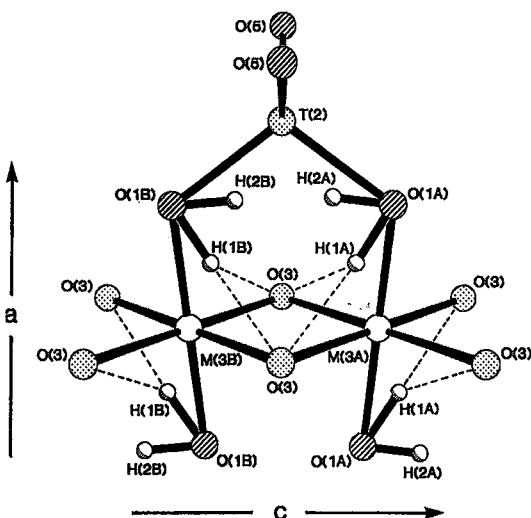


FIG. 5. The hydrogen positions in staurolite [coordinates from Ståhl *et al.* (1988), site nomenclature from Table 1, this study]. Hydrogen bonds are indicated by dashed lines; note that not all the positions indicated can be occupied simultaneously.

mirror plane parallel to (010) at $y = 0$, indicating that the Fe is actually positionally disordered into three nonequivalent sites within its tetrahedron of coordinating anions. Similar difference-Fourier maps also were presented by Bringham & Griffen (1986) and Ståhl *et al.* (1988). Alexander (1989) and Ståhl & Legros (1990) refined models with Fe occupying three closely spaced sites within the $T(2)$ tetrahedron. However, the authors of both studies were not satisfied with the results. Alexander (1989) noted the very high correlations and insignificant decrease in the R index, together with residual density in the difference-Fourier that "may indicate the presence of other (minor) occupied positions in the Fe tetrahedron in addition to the three previously observed subsites". Ståhl & Legros (1990) refined a very constrained three-site model (atoms at the apices of an equilateral triangle) and also refined an anharmonic displacement model for a central site; from model calculations, they concluded that the subsite separations are in the range 0.20–0.25 Å. Neither set of authors used the results of the subsite refinements in any quantitative crystal-chemical discussions, and it should perhaps be emphasized that this is quite correct; because of the obvious problem of resolution, it would be wrong to attach too much quantitative significance to the results of the split-site refinements.

Dyar *et al.* (1991) have assigned three doublets to Fe^{2+} at three different $T(2)$ subsites in the Mössbauer spectra of a wide variety of staurolite samples. In particular, these doublets were observed in synthetic Fe-rich staurolite, showing that the disorder cannot be entirely the result of solid-solution effects.

There have been various reasons suggested for this positional disorder, but there have also been insufficient crystallographic data on a wide range of compositions to see if the proposed mechanisms are of general applicability.

Order-disorder relations at $M(3A)$ and $M(3B)$

In the staurolite structure, within the oxide-hydroxide layer, adjacent octahedral sites in the $M(3)$ chain are symmetrically distinct, and are denoted $M(3A)$ and $M(3B)$, respectively. Náray-Szabó & Sasvári (1958) assigned all available Al to the $M(3A)$ site; thus $M(3A)$ was fully occupied, and $M(3B)$ was empty. Conversely, Hanisch (1966) refined the structure of a sample of zincian staurolite in the space group Ccm ; with this symmetry, $M(3A)$ and $M(3B)$ are symmetrically equivalent, and both sites were considered as half occupied. In perhaps the classic structural study of staurolite, Smith (1968) showed that (Al + Fe) is partly ordered between $M(3A)$ and $M(3B)$ in $C2/m$. Similar partial ordering over these sites has since been observed by Tagai & Joswig (1985), Bringham & Griffen (1986), Ståhl *et al.* (1988) and Alexander (1989), with the scattering power and assigned site-populations at $M(3A)$ always exceeding those at

$M(3B)$.

Ståhl & Legros (1990) illustrated a relationship between "occupancy" and mean bond-length at the $M(3A)$ and $M(3B)$ sites, two distinct correlations (by sample, not by site) being shown. They suggested the different correlations to be due to unspecified compositional differences between the samples. However, we note that they "normalized" the "occupancy" factors for each staurolite to "pure Fe" at the $T(2)$ site, and to (0.67 Al + 0.33 Mg) at the $M(3A)$ and $M(3B)$ sites. This procedure is unjustified by general stoichiometry of staurolite, and results in a range of "normalized occupancies" that is totally incompatible with the results of the present study.

Mechanism of substitution and disorder among cations

The chemical variations discussed above concern variations in cation proportions, and only in a few cases did the discussion focus on details of cation occupancy of specific sites. However, there have been many (commonly contradictory) proposals as to details of site populations in staurolite; these will be briefly outlined next.

Divalent cations: The principal substitutions proposed for staurolite are the homovalent substitutions $\text{Mg} \rightleftharpoons \text{Fe}^{2+}$, $\text{Zn} \rightleftharpoons \text{Fe}^{2+}$, and $\text{Co} \rightleftharpoons \text{Fe}^{2+}$. It has been shown by all structure-refinement studies that Fe^{2+} primarily (but not completely) occupies the tetrahedrally coordinated $T(2)$ site (albeit with some positional disorder), with subsidiary occupancy of the octahedrally coordinated $M(4A)$ and $M(4B)$ sites; Dyar *et al.* (1991) also suggested $M(3A)$ and $M(3B)$ as possible sites for $^{60}\text{Fe}^{2+}$. It was generally assumed that Mg, Zn and Co substitute for Fe^{2+} at the $T(2)$ site, and certainly the structural studies of Zn-bearing staurolite (Hanisch 1966) and Co-bearing staurolite (Bringham & Griffen 1986) show this to be dominantly the case. However, there have been many proposals for small amounts of Fe (commonly specified as Fe^{3+}) and Mg occupying the $M(1,2,3)$ sites, and small amounts of Al occurring at the $T(2)$ site. Indeed, from a statistical study of staurolite compositions, Griffen & Ribbe (1973) concluded that "the generally accepted view that Mg is the primary substituent for Fe at the Fe^{IV} site is not supported by the statistical analysis. It appears that Al and Zn (probably in that order) are more important substituents at the Fe^{IV} site". This conclusion was re-emphasized by Griffen *et al.* (1982), who made the following (admittedly simplified) assignments: all available Mg occupies the $M(3)$ sites; $M(1)$ and $M(2)$ are fully occupied by Al; the $T(2)$ site is fully occupied by (Fe + Zn + Al). However, it is apparent from Figure 3 that some degree of spurious correlation was introduced into these studies by the assumption that the formula unit contains 4 H atoms. Bringham & Griffen (1986) assigned *all* Mg (1.23 apfu) to the $M(1)$

and $M(3)$ sites in their refinement of a Co-bearing staurolite. Enami & Zang (1989) emphasized the importance of the preferential replacement of ^{61}Al by Mg, although they noted that $^{41}\text{Mg} \rightleftharpoons ^{41}\text{Fe}$ also seems to occur in some samples of high-Mg staurolite. On the other hand, Holdaway *et al.* (1986b) concluded that very little Mg replaces Al, but that a small amount of Al substituting for R^{2+} [presumably at the $T(2)$ or $M(4)$ sites] "cannot be excluded on the basis of our analytical results".

Trivalent and tetravalent cations: Staurolite contains small amounts of trivalent and tetravalent transition metals (Fe^{3+} , Ti^{4+} , Cr^{3+} , V^{3+}); their distribution over the cation sites is totally uncharacterized. It has generally been assumed that in staurolite, Fe^{3+} is octahedrally coordinated, although Tagai & Joswig (1985) did assign 0.24 Fe^{3+} apfu to the $T(1)$ site in their neutron-diffraction refinement of the structure. Ståhl *et al.* (1988) assigned 0.48 Fe^{3+} apfu to the $M(1)$ sites, whereas Alexander (1989) assigned 0.14 Fe^{3+} apfu to the $M(3)$ sites. Holdaway *et al.* (1986b) proposed significant $\text{Fe}^{3+} \rightleftharpoons \text{Al}$ substitution (0.30–0.35 apfu) in three of their staurolite samples; on the basis of size of cations, in octahedral coordination, they suggested that this occurs at $M(3A)$, but this argument is incorrect from a predictive point of view (polyhedral size is affected by the identity of the constituent cations, *not vice versa*). Bringhurst & Griffen (1986) assigned 0.20 Fe to $M(3)$ but did not specify its valence state.

Dyar *et al.* (1991) have thoroughly reviewed the literature on Mössbauer spectroscopy of staurolite. As with the structural and chemical studies reviewed above, there have been a number of different interpretations of essentially very similar data. They also examined a wide variety of samples of staurolite by Mössbauer spectroscopy, including several of those examined by us. With regard to Fe^{3+} , they concluded that the Fe^{3+} contents are usually low (~3% of total Fe) but can go up to 12% [in sample EH-6, suspected by Holdaway *et al.* (1986b) of having a high Fe^{3+} content]; they also suggested that Fe^{3+} is tetrahedrally coordinated, occurring at the $T(2)$ site.

With regard to Ti^{4+} , it is usually assumed to be octahedrally coordinated. However, on the basis of the observed pleochroism in staurolite, Ward (1984b) argued that it must occupy the $T(2)$ site in order to participate with ^{41}Fe in a $\text{Fe}^{2+} \rightleftharpoons \text{Ti}^{4+}$ charge-transfer reaction polarized strongly along the c axis. Normally, IVCT (InterValence Charge-Transfer) reactions are promoted by the close approach of the constituent cations, and must have an orbital path along which to propagate. This can involve metal–metal interaction *via* direct orbital-overlap across shared faces or edges of coordination polyhedra, or by metal – ligand – metal super-exchange. In both cases, the constituent cation polyhedra must share one or more ligands. In staurolite, the $T(2)$ tetrahedron does not link to neighboring $T(2)$ tetrahedra, indicating that $T(2)$ – $T(2)$

charge-transfer reactions are unlikely. Later, we propose an alternative site for Ti.

Other minor cations (Cr^{3+} , V^{3+}) are usually present in the range 0.01–0.10 apfu. They have been assigned to the $M(4)$ sites in several studies, but again there is no direct evidence for this; in this regard, note that the populations of the $M(4)$ sites are, by and large, so low that the sizes of the coordination polyhedra reflect the "size" of the vacant site rather than the occupied site.

Dyar *et al.* (1991) and Dutrow (1991) suggested that Li occurs at the $T(2)$ site because of the decrease in Fe with increasing Li in synthetic Li–Fe-bearing staurolite. The conclusion may be correct, but the reasoning is not; there could also be coupled $\square \rightleftharpoons \text{Fe}^{2+}$, $\text{Li} \rightleftharpoons \square$ substitutions at different structural sites. The question of where Li occurs in the structure must still be considered as open.

To summarize, there have been a large number of proposals for site-population patterns of different types; however, except for the principal substitutions $\text{Al} \rightleftharpoons \text{Si}$ at the $T(1)$ site and $\text{Zn} \rightleftharpoons \text{Fe}^{2+}$ and $\text{Co}^{2+} \rightleftharpoons \text{Fe}^{2+}$ at the $T(2)$ site, there is no systematic evidence for the general validity of these schemes.

EXPERIMENTAL METHODS

The provenance of the samples used in this work is indicated in Table 2. We tried to cover the entire observed compositional range of staurolite; specific analyzed samples were obtained from the authors of various published and unpublished studies to ensure this coverage. In particular, samples S(41) and S(42) are unique single crystals drilled from petrographic thin sections; the slightly lower quality of the data obtained is compensated by their very unusual chemical composition (Chopin, pers. comm.). All these particular samples were supplemented by staurolite samples of more usual compositions.

Collection of X-ray data

Crystals were selected for crystallographic measurement and collection of intensity data on the basis of optical clarity, freedom from inclusions, and equant shape. For the chemically well-characterized samples of Holdaway *et al.* (1986b), several crystals were examined from each mineral separate to check for sample homogeneity. All crystals were mounted on a Philips PW 1100 automated four-circle diffractometer and examined with graphite-monochromated $\text{MoK}\alpha$ X-radiation. Crystal quality was assessed *via* the profiles and widths of Bragg diffraction peaks; on this basis, several crystals were discarded. Diffraction data were measured only from those crystals judged to be of sufficiently good quality. Unit-cell dimensions were calculated by least-squares refinement of the d values obtained for 40 rows of reciprocal space by measuring the center of gravity of each reflection in the θ range

TABLE 2. PROVENANCE OF STAUROLITE CRYSTALS USED IN THIS WORK

Crystal	Sample code	Locality	References
S(1)	71-62R/1	Black Mtn., N.H.	M. Holdaway et al. (1986b)
S(2)	71-62R/6	Black Mtn., N.H.	"
S(3)	71-62R/5	Black Mtn., N.H.	"
S(4)	EH-6/6	Emery Hill, N.Y.	"
S(5)	EH-6/4	Emery Hill, N.Y.	"
S(6)	EH-6/2	Emery Hill, N.Y.	"
S(7)	3-3/1	West Sidney, Maine	"
S(8)	3-3/2	West Sidney, Maine	"
S(9)	106038/1	Franklin, N.C.	"
S(10)	106038/3	Franklin, N.C.	"
S(11)	117189/6	Stratford, N.C.	"
S(12)	117189/7	Stratford, N.C.	"
S(13)	117189/21	Stratford, N.C.	"
S(14)	117189/1	Stratford, N.C.	"
S(15)	6-3/1	East Winthrop, Maine	"
S(16)	6-3/2	East Winthrop, Maine	"
S(17)	WARD/7	Fiordland, New Zealand	C.M. Ward (1984a)
S(18)	MOT/2	unknown locality	A. Mottana, pers. comm.
S(19)	MUS/6-1	Pizzo Forno, Switzerland	This work
S(20)	MUS-AR/3	Pizzo Forno, Switzerland	"
S(21)	HP1/2	Pizzo Forno, Switzerland	"
S(22)	MUS/3	Pizzo Forno, Switzerland	"
S(23)	PIO/11	Brazil	"
S(24)	PIO/13	Brazil	"
S(25)	DW7/4	Antarctica	B. Lombardo, pers. comm.
S(26)	DW7/8II	Antarctica	"
S(27)	DER/10-2	Dervio, Italy	This work
S(28)	DER/2	Dervio, Italy	"
S(29)	DER/1	Dervio, Italy	"
S(30)	DER/10-4	Dervio, Italy	"
S(31)	MAR/FP15	Ticino river, Italy	"
S(32)	MAR/1	Ticino river, Italy	"
S(33)	MAR/15	Ticino river, Italy	"
S(34)	MAR/16	Ticino river, Italy	"
S(35)	MAR/5g	Ticino river, Italy	"
S(36)	MAR/2	Ticino river, Italy	"
S(37)	MAR/6-1	Ticino river, Italy	"
S(38)	MAR/8	Ticino river, Italy	"
S(39)	MAR/7II	Ticino river, Italy	"
S(40)	MAR/21	Ticino river, Italy	"
S(41)	85DM66b	Dora Maira, Italy	C. Chopin, pers. comm.
S(42)	BARR888	Barrhorn, Switzerland	"

2–35°, together with that of each “antireflection” at negative θ values. Refined cell-dimensions for the crystals used in the collection of the intensity data are given in Table 3. For the Zn-rich staurolite 117189 from Holdaway *et al.* (1986b), cell dimensions were measured on 14 different crystals.

Intensity data were collected for the monoclinic equivalents hkl and $h\bar{k}l$ in the range $2 < \theta < (30-65)^\circ$, depending on crystal size, using the step-scan profile technique of Lehmann & Larsen (1974). For all the crystals but S(4), S(19), S(20), S(23), S(24), S(29), S(32), S(33), S(37), S(38) and S(42), only intense reflections were collected beyond $\theta = 30^\circ$. Full details of the data-collection procedure are given in Ungaretti (1980) and Ungaretti *et al.* (1981). The intensity data were corrected for absorption by the method of North *et al.* (1968), corrected for Lorentz and polarization

effects, averaged and reduced to structure factors. A reflection is considered as observed if its intensity exceeds that of five standard deviations based on counting statistics.

Structure refinement

Fully ionized scattering-factors were used for the non-tetrahedrally coordinated cations, and both neutral and ionized scattering-factors were used for the tetrahedrally coordinated cations and the oxygen atoms (Ungaretti 1980). R indices are of the standard form, and are given as percentages.

All refinements were done in the space group $C2/m$, even where the equality of $I(hkl)$ and $I(\bar{h}kl)$ (together with $\beta = 90^\circ$ and the identity of the A and B sites) suggested orthorhombic $Ccmm$ symmetry. In particular,

TABLE 3. CELL DIMENSIONS (Å, Å³, °) AND MISCELLANEOUS STRUCTURE REFINEMENT INFORMATION FOR STAUROLITE

	S(1)	S(2)	S(3)	S(4)	S(5)	S(6)	S(7)	S(8)	S(9)	S(10)	S(11)	S(12)	S(13)	S(14)
<i>a</i>	7.863	7.863	7.865	7.879	7.882	7.881	7.874	7.873	7.878	7.877	7.868	7.868	7.868	7.869
<i>b</i>	16.613	16.612	16.608	16.624	16.622	16.625	16.625	16.627	16.606	16.606	16.610	16.609	16.609	16.606
<i>c</i>	5.650	5.650	5.651	5.661	5.660	5.661	5.662	5.663	5.657	5.657	5.658	5.658	5.659	5.659
β	90.09	90.14	90.23	90.00	90.01	90.06	90.02	90.04	90.08	90.09	90.03	90.13	90.27	90.45
<i>V</i>	738.1	738.1	738.1	741.5	741.6	741.7	741.3	741.2	740.0	740.0	739.5	739.4	739.6	739.5
θ_{\max}	45	45	45	32	45	45	45	45	45	45	45	45	45	45
<i>R</i> _{sym}	1.8	1.7	2.1	1.9	1.3	1.4	1.5	2.5	2.4	1.2	1.4	2.2	1.9	2.2
<i>R</i> _{obs}	1.7	1.7	1.8	1.8	1.8	1.7	1.9	1.8	2.5	1.6	2.0	2.1	1.9	1.8
<i>R</i> ₁₁₁	2.3	2.0	2.0	3.5	2.2	2.1	2.4	2.3	2.8	1.9	2.4	2.6	2.2	2.1
<i>N</i> _{obs}	1267	1957	1744	992	2037	1702	1653	1661	1989	1977	1760	1735	1991	1849
<i>N</i> _{tot}	1454	2162	1915	1339	2233	1904	1848	1847	2163	2138	1947	1939	2162	2024
	S(15)	S(16)	S(17)	S(18)	S(19)	S(20)	S(21)	S(22)	S(23)	S(24)	S(25)	S(26)	S(27)	S(28)
<i>a</i>	7.871	7.871	7.872	7.868	7.868	7.866	7.869	7.869	7.867	7.865	7.875	7.868	7.868	7.872
<i>b</i>	16.587	16.572	16.612	16.619	16.615	16.614	16.614	16.620	16.622	16.609	16.614	16.622	16.619	16.623
<i>c</i>	5.655	5.651	5.655	5.658	5.655	5.655	5.658	5.657	5.657	5.656	5.658	5.657	5.660	5.662
β	90.02	90.00	90.12	90.00	90.02	90.06	90.07	90.16	90.03	90.03	90.04	90.10	90.09	90.11
<i>V</i>	738.3	737.0	739.4	739.8	739.3	739.0	739.8	739.7	738.8	740.3	739.9	740.1	740.1	740.9
θ_{\max}	45	45	45	50	40	40	45	50	40	66	40	45	66	40
<i>R</i> _{sym}	1.8	2.4	2.0	2.3	1.7	1.2	1.9	1.1	1.4	1.8	1.2	1.6	1.1	1.7
<i>R</i> _{obs}	1.8	2.1	2.0	2.2	1.9	2.0	2.3	1.7	2.0	2.8	2.1	2.6	2.6	1.8
<i>R</i> ₁₁₁	2.5	2.8	2.4	2.5	2.9	2.8	2.7	2.1	2.9	4.3	2.4	2.7	2.7	2.1
<i>N</i> _{obs}	1320	1445	1628	2359	1840	1983	1941	1556	1904	5234	1580	2020	3782	1684
<i>N</i> _{tot}	1534	1687	1799	2500	2367	2364	2104	1706	2373	6722	1742	2187	3858	1855
	S(29)	S(30)	S(31)	S(32)	S(33)	S(34)	S(35)	S(36)	S(37)	S(38)	S(39)	S(40)	S(41)	S(42)
<i>a</i>	7.871	7.869	7.869	7.868	7.867	7.866	7.868	7.864	7.869	7.869	7.868	7.863	7.871	7.853
<i>b</i>	16.624	16.622	16.608	16.620	16.620	16.625	16.611	16.619	16.620	16.607	16.601	16.619	16.541	16.534
<i>c</i>	5.660	5.660	5.656	5.661	5.658	5.660	5.654	5.659	5.658	5.658	5.654	5.658	5.632	5.639
β	90.12	90.12	90.00	90.05	90.09	90.10	90.16	90.17	90.17	90.22	90.26	90.29	90.01	90.00
<i>V</i>	740.7	740.3	739.2	740.3	739.7	740.2	739.0	739.5	740.0	739.4	738.5	739.4	733.3	732.2
θ_{\max}	40	66	45	40	40	40	40	45	40	40	50	45	30	35
<i>R</i> _{sym}	1.9	1.1	1.4	2.4	1.3	3.4	1.6	1.9	1.6	2.3	2.9	2.8	5.8	3.3
<i>R</i> _{obs}	2.0	1.7	1.9	2.1	1.9	2.2	1.5	1.9	2.1	1.8	1.9	1.8	4.7*	2.2
<i>R</i> ₁₁₁	2.2	1.9	2.2	2.9	2.9	2.5	1.9	2.2	3.0	2.8	2.1	2.1	9.1	5.7
<i>N</i> _{obs}	1922	2734	1941	1949	1880	1724	1404	2112	1897	1922	2328	1663	652	919
<i>N</i> _{tot}	2382	2881	2105	2377	2376	1899	1582	2272	2374	2362	2435	1815	1113	1665

Note: e.s.d. < 0.002 Å for *a* and *c*, < 0.004 Å for *b* and < 0.02° for β

* refinement done on the reflections with $I \geq 3 \sigma(I)$

the crystals S(4), S(5), S(16), S(18), S(19) and S(31) were treated as monoclinic for both unit-cell and crystal-structure refinement in order to facilitate comparison across the whole series reported here and in the literature. For the structure refinements, the starting parameters were those of Smith (1968); the starting occupancies represented an average composition for staurolite. The refinements converged to *R* indices of ~2% for full-matrix refinement of all atomic positions, those site-occupancies considered as variable (see below, Table 5), and anisotropic displacement factors. At this stage, difference-Fourier maps showed the previously noted (Smith 1968, Alexander 1989, Ståhl & Legros 1990) three-lobed residual density around the T(2) site. We attempted to model this feature in our refinement; the details are given in the next section.

Modeling the disorder at the T(2) position: Although difference-Fourier maps show the characteristic three-lobed structure, Fourier maps calculated with a central

T(2) atom were not very informative. Consequently, refinement was initiated by displacing the three off-center sites a small amount from the central position, and dividing the aggregate scattering power at the central site equally among the three off-center sites. The starting *R*-index was high, but converged to a value slightly less than that for the central-site model. However, suspicious of the possibility of false minima, we repeated the procedure with a slightly different starting model; the refinement converged to a different geometrical solution with approximately the same *R*-index. Repeating this procedure several times produced a series of different solutions, all of which had about the same *R*-index. It is apparent that the solution obtained is dependent on the starting model, which indicates that most (if not all) of the solutions result from convergence to false minima.

In an effort to overcome this problem, we collected data on one crystal to very high resolution (maximum

TABLE 4. SELECTED INTERATOMIC DISTANCES (Å) FOR STAUROLITE

	S(1)	S(2)	S(3)	S(4)	S(5)	S(6)	S(7)	S(8)	S(9)	S(10)	S(11)	S(12)	S(13)	S(14)	S(15)	S(16)	S(17)	S(18)	S(19)	S(20)	S(21)	
T(1)-O2A	1.634	1.634	1.635	1.635	1.636	1.635	1.637	1.637	1.636	1.637	1.635	1.634	1.634	1.635	1.633	1.631	1.633	1.635	1.633	1.634	1.634	1.633
-O2B	1.634	1.634	1.635	1.634	1.636	1.636	1.636	1.636	1.636	1.636	1.634	1.634	1.633	1.634	1.630	1.631	1.632	1.635	1.633	1.633	1.633	1.633
-O3	1.648	1.650	1.653	1.655	1.655	1.655	1.656	1.655	1.658	1.658	1.653	1.652	1.654	1.651	1.654	1.655	1.652	1.655	1.651	1.651	1.651	1.651
-O4	1.644	1.644	1.646	1.642	1.642	1.641	1.644	1.643	1.644	1.641	1.641	1.643	1.643	1.642	1.641	1.640	1.642	1.642	1.642	1.642	1.642	1.641
<T(1)-O>	1.640	1.640	1.642	1.642	1.642	1.642	1.643	1.643	1.643	1.644	1.641	1.640	1.641	1.641	1.640	1.639	1.639	1.642	1.639	1.640	1.640	1.640
T(2)-O1A	2.055	2.055	2.057	2.016	2.016	2.019	2.029	2.032	2.022	2.022	2.016	2.013	2.015	2.011	2.034	2.040	2.028	2.035	2.035	2.033	2.033	2.034
-O1B	2.051	2.049	2.044	2.015	2.016	2.020	2.030	2.030	2.021	2.023	2.016	2.017	2.021	2.022	2.033	2.040	2.027	2.032	2.036	2.033	2.036	2.036
-O5	1.961	1.960	1.960	1.969	1.968	1.970	1.979	1.979	1.971	1.971	1.976	1.976	1.975	1.975	1.971	1.965	1.971	1.977	1.972	1.971	1.971	1.974
<T(2)-O>	2.007	2.006	2.005	1.992	1.992	1.995	2.004	2.005	1.996	1.997	1.996	1.996	1.996	1.996	2.002	2.003	1.999	2.005	2.004	2.002	2.002	2.005
M(1A)-O2A	1.937	1.937	1.935	1.948	1.949	1.946	1.945	1.943	1.943	1.942	1.942	1.941	1.936	1.932	1.943	1.945	1.941	1.942	1.944	1.941	1.941	1.943
-O4	1.898	1.898	1.895	1.899	1.899	1.897	1.898	1.899	1.898	1.897	1.898	1.897	1.895	1.893	1.901	1.903	1.899	1.898	1.900	1.898	1.898	1.899
-O5	1.892	1.891	1.892	1.907	1.908	1.905	1.899	1.898	1.900	1.901	1.899	1.899	1.897	1.897	1.889	1.886	1.896	1.897	1.895	1.896	1.896	1.896
<M(1A)-O>	1.909	1.909	1.907	1.918	1.919	1.916	1.914	1.913	1.914	1.913	1.913	1.912	1.910	1.909	1.911	1.911	1.912	1.912	1.913	1.912	1.912	1.913
M(1B)-O2B	1.938	1.940	1.942	1.949	1.948	1.950	1.945	1.945	1.946	1.946	1.944	1.944	1.949	1.954	1.946	1.946	1.948	1.942	1.943	1.943	1.943	1.944
-O4	1.901	1.902	1.903	1.899	1.899	1.901	1.899	1.900	1.899	1.900	1.900	1.901	1.903	1.905	1.903	1.903	1.902	1.899	1.899	1.899	1.900	1.901
-O5	1.892	1.891	1.891	1.905	1.907	1.908	1.898	1.899	1.905	1.903	1.901	1.908	1.903	1.903	1.889	1.884	1.899	1.896	1.895	1.896	1.896	1.896
<M(1B)-O>	1.910	1.911	1.912	1.918	1.918	1.920	1.915	1.915	1.917	1.916	1.915	1.915	1.918	1.921	1.913	1.911	1.916	1.912	1.912	1.912	1.913	1.915
M(2)-O1A	1.927	1.927	1.926	1.924	1.924	1.924	1.922	1.922	1.921	1.922	1.922	1.922	1.922	1.920	1.920	1.919	1.919	1.919	1.920	1.920	1.921	1.920
-O1B	1.925	1.924	1.924	1.926	1.925	1.923	1.922	1.922	1.923	1.923	1.922	1.922	1.923	1.925	1.930	1.921	1.920	1.921	1.922	1.920	1.921	1.919
-O2A	1.924	1.927	1.930	1.923	1.922	1.925	1.924	1.926	1.923	1.922	1.926	1.930	1.936	1.941	1.926	1.923	1.928	1.924	1.925	1.926	1.926	1.928
-O2B	1.917	1.915	1.911	1.923	1.922	1.919	1.924	1.924	1.917	1.918	1.924	1.924	1.917	1.908	1.925	1.922	1.920	1.925	1.925	1.922	1.922	1.923
-O3	1.869	1.869	1.873	1.878	1.880	1.879	1.878	1.878	1.880	1.880	1.873	1.874	1.875	1.879	1.887	1.889	1.877	1.874	1.874	1.874	1.875	1.875
-O5	1.868	1.868	1.869	1.869	1.869	1.868	1.867	1.868	1.867	1.867	1.867	1.868	1.869	1.869	1.859	1.856	1.867	1.867	1.868	1.868	1.868	1.866
<M(2)-O>	1.905	1.905	1.905	1.907	1.907	1.907	1.906	1.906	1.905	1.905	1.906	1.906	1.907	1.907	1.906	1.905	1.906	1.905	1.905	1.905	1.905	1.905
M(3A)-O1A	1.845	1.844	1.837	1.872	1.870	1.867	1.859	1.857	1.855	1.856	1.861	1.857	1.849	1.844	1.852	1.849	1.856	1.855	1.859	1.857	1.857	1.856
-O3	2.037	2.031	2.016	2.047	2.042	2.044	2.041	2.035	2.037	2.046	2.035	2.020	2.006	2.037	2.036	2.035	2.043	2.046	2.040	2.039	2.039	2.039
<M(3A)-O>	1.973	1.969	1.957	1.989	1.988	1.984	1.982	1.980	1.975	1.976	1.984	1.976	1.963	1.952	1.975	1.974	1.975	1.980	1.984	1.979	1.978	1.978
M(3B)-O1B	1.854	1.859	1.864	1.870	1.869	1.873	1.861	1.862	1.864	1.862	1.863	1.865	1.869	1.875	1.853	1.850	1.867	1.856	1.860	1.862	1.862	1.862
-O3	2.058	2.062	2.071	2.047	2.049	2.055	2.047	2.051	2.051	2.050	2.050	2.059	2.072	2.089	2.042	2.037	2.059	2.046	2.048	2.052	2.053	2.053
<M(3B)-O>	1.990	1.995	2.002	1.988	1.989	1.995	1.985	1.988	1.989	1.987	1.987	1.995	2.004	2.018	1.979	1.975	1.995	1.983	1.985	1.988	1.988	1.990
M(4A)-O1A	2.107	2.109	2.118	2.087	2.090	2.094	2.099	2.100	2.105	2.103	2.093	2.098	2.108	2.116	=	=	2.101	2.100	2.096	2.097	2.100	2.100
-O5	2.191	2.190	2.188	2.187	2.183	2.185	2.196	2.197	2.181	2.183	2.187	2.186	2.185	2.184	=	=	2.188	2.196	2.194	2.192	2.192	2.192
<M(4A)-O>	2.163	2.163	2.164	2.153	2.152	2.155	2.163	2.164	2.156	2.156	2.156	2.157	2.159	2.161	=	=	2.159	2.164	2.161	2.161	2.161	2.161
M(4B)-O1B	2.097	2.092	2.086	2.088	2.091	2.086	2.096	2.094	2.094	2.096	2.090	2.086	2.081	2.073	=	=	2.087	2.098	2.095	2.090	2.092	2.092
-O5	2.195	2.195	2.196	2.185	2.183	2.187	2.196	2.198	2.185	2.185	2.188	2.189	2.190	2.191	=	=	2.191	2.195	2.194	2.193	2.195	2.195
<M(4B)-O>	2.162	2.161	2.159	2.153	2.152	2.153	2.163	2.163	2.155	2.155	2.156	2.156	2.153	2.152	=	=	2.156	2.163	2.161	2.159	2.161	2.161
<M(1)-O>	1.909	1.910	1.910	1.918	1.918	1.918	1.914	1.914	1.915	1.914	1.914	1.913	1.914	1.914	1.912	1.911	1.914	1.912	1.912	1.912	1.912	1.914
<M(3)-O>	1.981	1.982	1.979	1.988	1.988	1.989	1.983	1.984	1.982	1.981	1.985	1.985	1.985	1.985	1.977	1.974	1.985	1.981	1.984	1.984	1.984	1.984
<M(4)-O>	2.162	2.162	2.161	2.153	2.152	2.154	2.163	2.163	2.155	2.155	2.156	2.155	2.156	2.157	=	=	2.157	2.163	2.161	2.160	2.161	2.161

Note: e. s. d. are ≤ 0.002 Å.

$2\theta = 135^\circ$, 5234 unique reflections). The problem of false minima still persisted, and we also concluded that the $T(2)$ - $T(2)$ separations obtained from the three-site models depend on the resolution of the X-ray data used in the refinement. The minimum possible interplanar spacing allowed by the very high-resolution data is $d_{\min} = \lambda/2 \sin \theta_{\max} = 0.38$ Å, and the minimum separation that can be reliably imaged in a map of electron density is $0.715 d_{\min} = 0.27$ Å. Thus we conclude that the real $T(2)$ - $T(2)$ separations are less than 0.27 Å, and hence they can only be adequately resolved with a radiation of considerably shorter wavelength than $\text{MoK}\alpha$. This is in accord with the separations estimated by Ståhl & Legros (1990) from the magnitudes of the central-site isotropic displacement factors.

The following procedure was used to cope with this problem. A central $T(2)$ site was used, and the occupancy and thermal parameters were refined un-

constrained. Upon convergence, small amounts of scattering were added at the three subsidiary positions corresponding to the familiar lobes in the difference-Fourier, and the model was refined to convergence. We emphasize that the three subsidiary positions have no stereochemical significance except to indicate that one (or more) disordered positions of the cations lies along each vector joining the position of the central cation to the subsidiary positions, as assumed in all previous work. However, we found that the total scattering from the $T(2)$ site (or aggregate scattering from the central site and subsites) was the same in the one-site model, the three-site model (without the central site), and the four-site model; it is apparent that the additional density added at the three subsidiary positions was accompanied by a decrease in the displacement factor at the central site and a corresponding decrease in the density at the central site, with a net change in scattering of zero. For simplicity, we give

TABLE 4. CONTINUED.

	S(22)	S(23)	S(24)	S(25)	S(26)	S(27)	S(28)	S(29)	S(30)	S(31)	S(32)	S(33)	S(34)	S(35)	S(36)	S(37)	S(38)	S(39)	S(40)	S(41)	S(42)
T(1)-02A	1.634	1.633	1.633	1.633	1.634	1.634	1.636	1.636	1.635	1.635	1.634	1.633	1.635	1.635	1.632	1.633	1.633	1.634	1.634	1.631	1.630
-02B	1.633	1.634	1.633	1.633	1.634	1.634	1.635	1.634	1.634	1.635	1.635	1.633	1.633	1.634	1.633	1.635	1.632	1.634	1.634	1.630	1.631
-03	1.654	1.654	1.653	1.650	1.651	1.654	1.655	1.655	1.655	1.655	1.653	1.651	1.652	1.652	1.651	1.652	1.651	1.655	1.652	1.652	1.649
-04	1.641	1.643	1.642	1.641	1.642	1.641	1.643	1.644	1.641	1.643	1.642	1.641	1.642	1.643	1.641	1.643	1.641	1.645	1.642	1.644	1.637
<T(1)-0>	1.641	1.641	1.640	1.640	1.640	1.641	1.642	1.642	1.641	1.642	1.641	1.640	1.640	1.641	1.639	1.641	1.639	1.642	1.641	1.639	1.637
T(2)-01A	2.035	2.028	2.032	2.040	2.039	2.036	2.037	2.034	2.038	2.029	2.030	2.035	2.033	2.040	2.035	2.031	2.028	2.025	2.034	2.016	2.007
-01B	2.037	2.029	2.031	2.040	2.040	2.035	2.037	2.031	2.036	2.026	2.029	2.035	2.031	2.038	2.033	2.031	2.032	2.029	2.029	2.025	2.005
-05	1.975	1.977	1.976	1.971	1.972	1.977	1.976	1.978	1.976	1.974	1.979	1.975	1.978	1.968	1.978	1.975	1.972	1.971	1.977	1.943	1.961
<T(2)-0>	2.005	2.003	2.004	2.005	2.006	2.006	2.006	2.005	2.006	2.001	2.004	2.005	2.005	2.004	2.006	2.003	2.001	1.999	2.004	1.982	1.983
M(1A)-02A	1.940	1.943	1.942	1.944	1.940	1.941	1.942	1.941	1.942	1.942	1.942	1.941	1.939	1.937	1.938	1.939	1.938	1.936	1.935	1.940	1.935
-04	1.896	1.899	1.898	1.898	1.898	1.898	1.898	1.897	1.899	1.898	1.898	1.900	1.900	1.897	1.897	1.897	1.897	1.895	1.896	1.904	1.903
-05	1.896	1.896	1.896	1.897	1.895	1.895	1.897	1.897	1.896	1.897	1.896	1.896	1.895	1.894	1.894	1.895	1.894	1.894	1.893	1.897	1.888
<M(1A)-0>	1.911	1.913	1.912	1.913	1.911	1.911	1.912	1.911	1.912	1.913	1.912	1.912	1.911	1.910	1.910	1.910	1.910	1.909	1.908	1.914	1.909
M(1B)-02B	1.948	1.943	1.942	1.946	1.945	1.947	1.947	1.947	1.947	1.943	1.945	1.944	1.944	1.944	1.947	1.946	1.949	1.946	1.950	1.943	1.935
-04	1.900	1.899	1.898	1.900	1.903	1.901	1.901	1.900	1.901	1.897	1.900	1.901	1.901	1.902	1.903	1.902	1.905	1.902	1.904	1.896	1.902
-05	1.898	1.897	1.896	1.898	1.896	1.897	1.898	1.898	1.898	1.899	1.899	1.899	1.899	1.896	1.897	1.899	1.894	1.898	1.900	1.890	1.886
<M(1B)-0>	1.916	1.913	1.912	1.915	1.915	1.915	1.915	1.915	1.915	1.913	1.915	1.913	1.915	1.914	1.916	1.916	1.918	1.915	1.918	1.910	1.908
M(2)-01A	1.922	1.921	1.920	1.923	1.923	1.921	1.923	1.922	1.922	1.919	1.920	1.921	1.918	1.923	1.919	1.921	1.920	1.920	1.919	1.920	1.922
-01B	1.923	1.921	1.921	1.923	1.923	1.923	1.924	1.925	1.923	1.921	1.920	1.922	1.918	1.923	1.918	1.923	1.924	1.923	1.918	1.916	1.924
-02A	1.928	1.926	1.925	1.926	1.929	1.928	1.927	1.928	1.927	1.923	1.928	1.929	1.932	1.928	1.935	1.933	1.933	1.933	1.938	1.912	1.919
-02B	1.916	1.924	1.923	1.922	1.919	1.921	1.920	1.919	1.921	1.922	1.925	1.923	1.926	1.917	1.921	1.918	1.917	1.915	1.914	1.917	1.918
-03	1.876	1.876	1.875	1.872	1.872	1.876	1.877	1.877	1.876	1.878	1.876	1.873	1.874	1.874	1.875	1.875	1.877	1.877	1.877	1.877	1.873
-05	1.867	1.867	1.866	1.869	1.869	1.866	1.868	1.867	1.865	1.867	1.868	1.868	1.868	1.868	1.868	1.869	1.866	1.868	1.867	1.865	1.861
<M(2)-0>	1.905	1.906	1.905	1.906	1.906	1.906	1.906	1.906	1.906	1.905	1.906	1.906	1.906	1.905	1.906	1.906	1.906	1.906	1.906	1.901	1.903
M(3A)-01A	1.849	1.857	1.851	1.857	1.853	1.850	1.853	1.852	1.848	1.857	1.857	1.853	1.853	1.847	1.848	1.850	1.849	1.843	1.840	1.875	1.845
-03	2.028	2.043	2.040	2.043	2.036	2.034	2.035	2.032	2.032	2.042	2.041	2.038	2.036	2.029	2.027	2.029	2.025	2.015	2.013	2.035	2.035
<M(3A)-0>	1.968	1.981	1.977	1.981	1.975	1.972	1.974	1.972	1.971	1.980	1.980	1.976	1.975	1.968	1.968	1.969	1.967	1.958	1.955	1.982	1.972
M(3B)-01B	1.865	1.859	1.854	1.863	1.862	1.860	1.863	1.865	1.861	1.859	1.862	1.861	1.864	1.863	1.867	1.868	1.868	1.866	1.874	1.856	1.848
-03	2.060	2.047	2.048	2.053	2.061	2.056	2.055	2.057	2.044	2.051	2.056	2.058	2.062	2.065	2.066	2.067	2.069	2.077	2.035	2.041	
<M(3B)-0>	1.995	1.984	1.983	1.989	1.995	1.991	1.991	1.993	1.992	1.982	1.988	1.991	1.993	1.996	1.999	2.000	2.001	2.001	2.009	1.975	1.976
M(4A)-01A	2.107	2.097	2.102	2.101	2.103	2.106	2.105	2.105	2.108	2.098	2.098	2.102	2.101	2.108	2.106	2.106	2.108	2.114	2.115	2.079	2.099
-05	2.195	2.195	2.193	2.193	2.193	2.196	2.196	2.196	2.196	2.191	2.196	2.195	2.189	2.196	2.192	2.188	2.184	2.192	2.162	2.170	
<M(4A)-0>	2.165	2.162	2.163	2.162	2.163	2.166	2.166	2.166	2.166	2.160	2.163	2.164	2.164	2.162	2.166	2.163	2.161	2.160	2.166	2.134	2.146
M(4B)-01B	2.088	2.094	2.098	2.095	2.091	2.092	2.092	2.089	2.092	2.095	2.092	2.092	2.089	2.089	2.084	2.084	2.083	2.084	2.075	2.100	2.096
-05	2.198	2.195	2.194	2.195	2.197	2.199	2.198	2.199	2.198	2.191	2.198	2.197	2.199	2.195	2.200	2.197	2.194	2.191	2.200	2.155	2.168
<M(4B)-0>	2.162	2.161	2.162	2.161	2.162	2.163	2.162	2.162	2.163	2.159	2.163	2.162	2.162	2.159	2.161	2.159	2.162	2.155	2.158	2.137	2.144
<M(1)-0>	1.913	1.913	1.912	1.914	1.913	1.913	1.913	1.913	1.913	1.913	1.913	1.913	1.913	1.912	1.913	1.913	1.914	1.912	1.913	1.912	1.908
<M(3)-0>	1.981	1.982	1.980	1.985	1.985	1.981	1.982	1.982	1.981	1.981	1.984	1.983	1.984	1.982	1.983	1.984	1.984	1.979	1.982	1.978	1.974
<M(4)-0>	2.163	2.161	2.162	2.161	2.162	2.164	2.164	2.164	2.164	2.159	2.163	2.163	2.163	2.160	2.163	2.161	2.159	2.157	2.162	2.135	2.145

the central-site results only.

Full-matrix refinement of all variables converged to final *R*-indices in the range 1–2%. Atomic coordinates and displacement parameters may be obtained from the Depository of Unpublished Data, CISTI, National Research Council of Canada, Ottawa, Ontario K1A 0S2, selected interatomic distances are given in Table 4, and site-scattering data are listed in Table 5.

Electron-microprobe analysis

Subsequent to the experimental crystallographic work, some of the crystals used in the collection of the X-ray-diffraction data were analyzed by electron- and ion-microprobe techniques. The crystals were mounted in piccolite in small holes in 2.54 cm diameter copper discs; each disc also contained several crystals of staurolite 71–62R and EH–6 (Holdaway *et al.* 1986b) as a check on mount-to-mount compatibility. The discs were polished and subsequently carbon-coated.

Electron-microprobe analyses were done on a fully automated Cameca SX–50 operating in the wavelength-dispersion mode with the following conditions: excitation voltage: 15 kV; specimen current: 20 nA; peak count time: 20 s; background count time: 10 s. The following standards and crystals were used for *K*α X-ray lines: Al: Al₂O₃, TAP; Fe: fayalite, LiF; Si: diopside, PET; Mg: MgO, TAP; Zn: gahnite, LiF; F: fluor-riebeckite, TAP; Mn: tephroite, LiF; Ti: titanite, LiF; Cr: chromite, LiF; Co: cobaltite, LiF. Each grain was analyzed at a minimum of 12 points (commonly twice this number, depending on the size of the exposed surface) to check for compositional zoning and to get a representative composition for the whole crystal used in the diffraction experiment. In addition, samples 71–62R and EH–6 were analyzed on all five probe mounts to check for consistency of analytical conditions; no significant differences from mount to mount were observed. Data reduction was done with the φ(ρZ) method (Pouchou & Pichoir 1984, 1985),

TABLE 5. REFINED SCATTERING POWERS* (PFU) IN STAUROLITE CRYSTALS

	N**	S(1)	S(2)	S(3)	S(4)	S(5)	S(6)	S(7)	S(8)	S(9)	S(10)	S(11)	S(12)	S(13)	S(14)
M(1A)	4	52.7	52.5	52.8	53.1	52.3	52.7	52.8	52.6	51.8	52.1	52.3	52.4	52.6	52.7
M(1B)	4	52.8	52.5	52.5	53.1	52.2	52.7	52.7	52.4	52.2	52.1	52.2	52.2	52.3	52.5
M(2)	8	106.5	105.8	105.1	106.7	105.2	106.0	106.1	105.3	106.0	104.9	105.4	105.2	106.4	107.2
M(3A)	2	13.9	14.9	17.4	13.4	13.7	14.6	13.9	14.1	14.6	14.4	12.9	15.1	17.8	21.5
M(3B)	2	9.8	8.8	7.1	13.4	13.4	12.3	12.7	12.3	11.5	11.9	12.2	10.3	7.8	4.3
M(4A)	2	7.2	7.5	9.0	1.5	1.5	1.5	1.3	1.5	1.8	2.0	1.4	1.9	2.0	2.5
M(4B)	2	3.9	3.0	1.7	1.6	1.4	1.3	1.1	1.1	1.6	1.5	1.3	0.8	0.3	0.1
T(2)	4	71.3	70.6	71.9	86.4	84.9	86.0	92.3	91.3	89.8	90.7	103.4	102.6	103.9	102.9
	N**	S(15)	S(16)	S(17)	S(18)	S(19)	S(20)	S(21)	S(22)	S(23)	S(24)	S(25)	S(26)	S(27)	S(28)
M(1A)	4	52.8	53.4	52.9	52.8	52.2	52.2	52.3	52.0	52.3	52.4	52.5	53.0	52.2	52.5
M(1B)	4	52.8	53.4	52.7	52.9	52.1	52.4	52.3	52.0	52.3	52.3	52.4	53.0	52.0	52.5
M(2)	8	106.4	106.8	107.0	105.3	105.3	104.0	108.8	105.2	106.9	105.2	106.3	107.9	104.4	105.5
M(3A)	2	13.4	13.3	15.2	13.1	13.0	13.9	14.1	16.1	13.4	13.5	13.6	14.9	14.9	15.0
M(3B)	2	12.5	13.0	11.0	12.9	12.6	11.8	11.4	9.7	12.5	12.5	11.7	10.2	11.0	11.1
M(4A)	2	=	=	3.0	1.7	2.8	2.5	2.8	2.6	1.9	2.0	2.9	4.1	2.0	2.5
M(4B)	2	=	=	1.9	1.9	2.5	2.0	2.3	1.0	1.6	1.6	2.4	2.1	1.2	1.5
T(2)	4	78.1	72.6	77.0	90.1	82.5	83.2	85.9	90.2	88.2	87.7	86.5	84.3	91.4	90.0
	N**	S(29)	S(30)	S(31)	S(32)	S(33)	S(34)	S(35)	S(36)	S(37)	S(38)	S(39)	S(40)	S(41)	S(42)
M(1A)	4	52.5	52.1	51.9	52.5	52.8	52.7	52.5	52.5	53.1	53.0	52.2	53.3	52.9	52.4
M(1B)	4	52.2	51.8	51.9	52.6	52.6	52.8	52.4	52.3	53.0	53.0	52.3	53.2	53.5	52.6
M(2)	8	106.5	104.6	104.8	106.9	107.1	107.0	106.6	106.4	105.9	106.6	105.3	107.4	105.4	106.0
M(3A)	2	15.4	15.2	13.1	13.9	14.5	14.8	16.0	16.2	16.6	17.2	18.1	19.0	12.8	12.6
M(3B)	2	10.7	10.8	12.8	12.1	11.1	11.1	9.4	9.4	9.2	8.8	7.8	7.1	13.0	11.5
M(4A)	2	2.2	2.3	1.8	1.6	3.0	2.7	4.4	2.8	2.9	2.5	3.9	3.2	6.2	2.8
M(4B)	2	1.1	1.2	1.7	1.4	2.1	2.0	1.9	1.1	1.1	0.8	1.0	0.5	6.2	2.5
T(2)	4	91.2	90.7	88.1	91.7	85.9	89.3	79.8	88.1	86.9	85.1	87.1	87.7	25.2	81.1

* e.s.d. are 0.1-0.4 electrons

** N is the number of times this site occurs in the structural formula

and the resultant mean composition for each grain is given in Table 7. Crystals S(41) and S(42) were analyzed by electron- and ion-microprobe methods in Paris by C. Chopin (pers. comm.); results are given in Table 6.

Several of the samples examined here were previously analyzed by Holdaway *et al.* (1986b). Table 7 provides a comparison of the compositions of grains from the same mineral separates; the agreement is excellent, and as both different instruments, sets of standards, and standardization and correction procedures were used (Bence-Albee method by Holdaway *et al.* 1986b; $\phi(\rho Z)$ method in this work), the agreement is indicative of accurate analyses.

Ion-microprobe analysis

Ion-microprobe analyses were done on a Cameca IMS 4F according to the method of Ottolini *et al.* (1992, 1993). Both ion-microprobe and crystal-chemical results suggested that the Li_2O content of sample 6-3 given by Holdaway *et al.* (1986b) was overestimated by at least 20%. This sample was re-analyzed by Holdaway (pers. comm., 1991), with a resultant value of 0.99 wt% Li_2O that agrees exactly with the ion-microprobe result (Table 7).

Normalization of the formula unit

The correct way of calculating the formula unit of staurolite is on the basis of 48 (O,OH,F), including Li_2O contents. Such unit formulae are available for the staurolite samples obtained from Holdaway *et al.* (1986b), but not for the remainder of the samples, as the paucity of material in most cases precluded analysis for H_2O (F was not a significant component in any of the staurolite samples analyzed). In the absence of such analytical data, Holdaway *et al.* (1986b) suggested following schemes of renormalization: (1) a basis of 46.47 O (*i.e.*, H = 3.06 apfu), with Li = 0.2 apfu for staurolite that coexists with garnet or biotite; (2) a basis of 45.93 O (*i.e.*, 4.14 H apfu) for staurolite that does not coexist with garnet or biotite; (3) a basis of 25.53 (Al + Si) for staurolite forming under very reducing conditions, and coexisting with graphite and hematite-free ilmenite. For those cases for which we do not have H concentrations, we have renormalized the unit formulae on the basis of 46.5 O (= 3.0 H apfu) with the determined Li_2O values, similar to the first method suggested by Holdaway *et al.* (1986b). We can be sure that none of these samples have H \approx 4 apfu because of our site-scattering refinement results, as there are several features of H-rich staurolite [high M(4) scattering, low M(3) scattering] that differ signif-

TABLE 6. RESULTS OF ELECTRON AND ION MICROPROBE ANALYSES* AND UNIT FORMULAE** OF STAUROLITE CRYSTALS

	S(1) [23]	S(2) [25]	S(3) [23]	S(4) [25]	S(5) [23]	S(6) [24]	S(7) [24]	S(8) [24]	S(9) [24]	S(10) [23]	S(12) [26]	S(13) [12]	S(15) [23]	S(16) [24]	S(17) [24]	S(18) [12]
SiO ₂ , wt%	27.57	27.83	27.82	27.90	27.64	27.78	27.25	27.05	26.75	26.48	27.16	27.19	28.16	28.40	27.48	26.21
Al ₂ O ₃	54.85	55.12	54.91	53.20	53.36	53.15	53.99	53.82	54.74	54.66	52.96	52.64	54.99	55.36	54.23	54.30
TiO ₂	0.42	0.35	0.32	0.37	0.37	0.39	0.41	0.41	0.33	0.27	0.48	0.41	0.45	0.43	0.54	0.47
Cr ₂ O ₃	0.03	0.03	0.01	0.03	0.05	0.04	0.04	0.03	0.01	0.01	0.03	0.03	0.05	0.06	0.03	0.02
Fe ₂ O ₃	0.43	0.42	0.43	1.71	1.70	1.71	0.46	0.47	0.35	0.35	0.42	0.42	0.61	0.62	0.39	0.48
FeO	12.40	12.21	12.39	11.31	11.18	11.26	13.46	13.67	10.05	10.24	9.03	8.99	10.39	10.55	11.33	13.89
MgO	0.67	0.66	0.62	3.92	4.07	3.98	1.85	1.69	2.67	2.55	1.77	1.88	0.87	0.91	3.41	1.65
MnO	0.22	0.22	0.22	0.16	0.13	0.14	0.44	0.50	0.36	0.34	0.13	0.11	0.50	0.49	0.09	0.18
CoO	0.01	0.02	0.02	0.04	0.04	0.03	0.02	0.02	0.01	0.02	0.02	0.01	0.03	0.03	0.01	0.01
ZnO	0.13	0.20	0.19	0.30	0.28	0.26	0.20	0.21	3.11	3.13	6.39	6.71	0.53	0.43	0.13	0.14
Li ₂ O	0.36	0.36	0.36	0.02	0.01	0.02	0.08	0.14	0.01	0.01	0.05	0.05	0.92	1.04	0.02	0.07
H ₂ O	(2.26)	(2.26)	(2.26)	(1.52)	(1.52)	(1.53)	(1.43)	(1.43)	(1.62)	(1.62)	(1.65)	(1.65)	(1.80)	(1.80)	-	-
Sum	99.35	99.68	99.55	100.48	100.35	100.29	99.63	99.44	100.01	99.68	100.09	100.09	99.30	100.12	97.66	97.42
Si	7.641	7.679	7.693	7.733	7.669	7.713	7.666	7.636	7.483	7.441	7.677	7.698	7.784	7.784	7.656	7.424
Al	0.359	0.321	0.307	0.267	0.331	0.287	0.334	0.364	0.517	0.559	0.323	0.302	0.216	0.216	0.344	0.576
Sum	8.000	8.000	8.000	8.000	8.000	8.000	8.000	8.000	8.000	8.000	8.000	8.000	8.000	8.000	8.000	8.000
Al	17.559	17.605	17.589	17.112	17.118	17.105	17.568	17.543	17.530	17.545	17.320	17.262	17.700	17.668	17.463	17.551
Cr	0.007	0.007	0.002	0.007	0.011	0.009	0.009	0.007	0.002	0.002	0.007	0.007	0.011	0.013	0.007	0.004
Ti	0.088	0.073	0.067	0.077	0.077	0.081	0.087	0.087	0.069	0.057	0.102	0.087	0.094	0.089	0.113	0.100
Fe ³⁺	0.090	0.087	0.089	0.357	0.355	0.357	0.097	0.100	0.074	0.074	0.089	0.089	0.127	0.128	0.082	0.102
Fe ²⁺	2.874	2.818	2.865	2.622	2.594	2.615	3.167	3.227	2.351	2.407	2.135	2.128	2.402	2.418	2.640	3.290
Mg	0.277	0.272	0.256	1.620	1.683	1.647	0.776	0.711	1.113	1.068	0.746	0.793	0.359	0.372	1.416	0.697
Mn	0.052	0.051	0.052	0.038	0.031	0.033	0.105	0.120	0.085	0.081	0.031	0.026	0.117	0.114	0.021	0.043
Zn	0.027	0.041	0.039	0.061	0.057	0.053	0.042	0.044	0.642	0.649	1.334	1.403	0.108	0.087	0.027	0.029
Co	0.002	0.004	0.004	0.009	0.009	0.007	0.005	0.005	0.002	0.005	0.005	0.002	0.007	0.007	0.002	0.002
Li	0.401	0.400	0.400	0.022	0.011	0.022	0.091	0.159	0.011	0.011	0.057	0.057	1.023	1.146	0.022	0.080
Catsum	29.377	29.358	29.363	29.925	29.946	29.929	29.946	30.003	29.879	29.899	29.826	29.854	29.948	30.042	29.793	29.898
H	4.178	4.160	4.169	2.810	2.813	2.815	2.684	2.693	3.023	3.037	3.111	3.116	3.319	3.291	(3)	(3)

* Fe₂O₃ values are taken from Dyar *et al.* (1991) where available; all others are estimated as 3% of the total Fe as found by Dyar *et al.* (1991) for most staurolite crystals; H₂O values are taken from Holdaway *et al.* (1986a).

** staurolite crystals S(1)-S(16) normalized on the basis of 48(O,H,F); staurolite crystals S(17)-S(40) normalized on 46.5 O.

* values in [] are the number of analyses on each crystal.

icantly from those of normal staurolite. Unit formulae are given in Table 6.

Renormalization on the basis of 46.5 O obviously introduces some error into the formula unit. Recalculation of the analytical data of Holdaway *et al.* (1986b) on the basis of 46.5 O gives an idea of the magnitude of the errors so introduced. These are negligible except for Al and Si, by far the most abundant cations in the structure. Consequently, for correlations involving Si and Al, only the staurolite samples obtained from Holdaway *et al.* (1986b) generally were used, whereas for correlations involving other cations, all data were used.

SITE POPULATIONS: GENERAL CONSIDERATIONS

The assignment of site populations is a very complicated problem in staurolite, and here we define the procedure that we use. During structure refinement, the occupancy of each cation site was set as $xM + (1-x)N$, where M and N are the principal (possible) scattering species at that site [e.g., $M = \text{Al}$, $N = \text{Fe}$ for $M(2)$, $M = \text{Al}$, $N = \square$ for $M(3A)$ and $M(3B)$]. However, in complex solid-solutions, the resultant *site-occupan-*

cies do not necessarily represent exactly what atoms are at the site; in fact, they only give the amount of X-ray scattering from the site, and we prefer to refer to this procedure as site-scattering refinement. We have found it clearer and more convenient to express the results of the site-scattering refinement in terms of the *site-scattering power*, the number of electrons associated with the atoms at that site in the structural formula. These electrons may then be assigned to (or associated with) specific chemical species on the basis of known chemistry and *via* stereochemical analysis. These scattering powers were converted into epfu (electrons per formula unit) by taking into account Z and the site multiplicities for the $C2/m$ space group. When the site-scattering powers are converted into chemical species, this gives the *site populations*, which do not necessarily sum to unity, but sum to the number of equivalent sites in the corresponding structural formula.

The dominant X-ray scattering species in staurolite (besides O) are Al, Si, Mg and Fe. As Al, Si and Mg all scatter X rays in a very similar fashion, they cannot be differentiated directly by their X-ray scattering power. At some stages in the assignment of site populations, we will group species of similar scattering

TABLE 6. CONTINUED.

	S(20)	S(22)	S(23)	S(24)	S(25)	S(26)	S(27)	S(30)	S(33)	S(35)	S(36)	S(39)	S(40)	[§] S(41)	[§] S(42)
	[12]	[12]	[12]	[12]	[12]	[24]	[24]	[12]	[12]	[12]	[12]	[24]	[12]	-	-
SiO ₂ wt%	27.01	26.93	26.59	26.64	27.07	26.93	26.59	26.59	26.79	26.98	27.32	27.03	27.84	30.66	28.49
Al ₂ O ₃	55.02	54.04	54.48	54.45	53.32	53.90	53.77	53.97	53.75	54.70	55.49	54.21	54.32	57.45	54.12
TiO ₂	0.49	0.52	0.46	0.49	0.36	0.36	0.33	0.34	0.60	0.52	0.55	0.58	0.49	0.18	0.11
Cr ₂ O ₃	0.02	0.01	0.02	0.02	0.02	0.02	0.02	0.02	0.02	0.01	0.04	0.06	0.03	-	-
Fe ₂ O ₃	0.44	0.44	0.44	0.45	0.44	0.42	0.49	0.49	0.46	0.41	0.45	0.36	0.46	-	-
FeO	12.87	12.77	12.94	13.01	12.78	12.36	14.20	14.19	13.28	11.98	12.98	10.63	13.32	0.72	1.40
MgO	2.32	2.19	1.96	2.03	1.94	1.77	1.66	1.66	1.74	1.76	1.60	1.73	1.68	7.77	0.45
MnO	0.20	0.26	0.35	0.33	0.22	0.25	0.14	0.15	0.15	0.37	0.16	0.38	0.18	-	0.01
CoO	0.02	0.02	0.02	0.03	0.04	0.03	0.04	0.02	0.02	0.02	0.03	0.01	0.02	-	-
ZnO	0.29	0.55	0.37	0.37	0.94	1.06	0.12	0.12	0.43	0.48	0.21	2.58	0.14	0.10	11.82
Li ₂ O	0.07	0.09	0.09	0.08	0.11	0.11	0.10	0.10	0.10	0.12	-	0.14	0.17	0.90	0.45
H ₂ O	-	-	-	-	-	-	-	-	-	-	-	-	-	-	-
Sum	98.75	97.82	97.72	97.90	97.24	97.21	97.46	97.65	97.34	97.35	98.83	97.71	98.65	97.78	96.85
Si	7.507	7.568	7.484	7.487	7.667	7.617	7.534	7.518	7.577	7.581	7.576	7.607	7.740	7.958	7.97
Al	0.493	0.432	0.516	0.513	0.333	0.383	0.466	0.482	0.423	0.419	0.424	0.393	0.260	0.042	0.03
Sum	8.000	8.000	8.000	8.000	8.000	8.000	8.000	8.000	8.000	8.000	8.000	8.000	8.000	8.000	8.000
Al	17.530	17.468	17.556	17.523	17.466	17.586	17.491	17.503	17.494	17.696	17.713	17.588	17.538	17.534	17.83
Cr	0.004	0.002	0.004	0.004	0.004	0.002	0.004	0.004	0.004	0.002	0.009	0.013	0.007	-	-
Ti	0.102	0.110	0.097	0.104	0.077	0.077	0.070	0.072	0.128	0.110	0.115	0.123	0.102	0.035	0.02
Fe ³⁺	0.092	0.093	0.093	0.095	0.094	0.089	0.104	0.104	0.098	0.087	0.094	0.076	0.096	-	-
Fe ²⁺	2.991	3.001	3.046	3.058	3.027	2.924	3.365	3.355	3.141	2.815	3.010	2.502	3.097	0.156	0.33
Mg	0.961	0.917	0.822	0.851	0.819	0.746	0.701	0.700	0.734	0.737	0.661	0.726	0.696	3.007	0.19
Mn	0.047	0.062	0.083	0.079	0.053	0.060	0.034	0.036	0.036	0.088	0.038	0.091	0.042	-	-
Zn	0.060	0.114	0.077	0.077	0.197	0.221	0.025	0.025	0.090	0.100	0.043	0.536	0.029	0.019	2.45
Co	0.004	0.005	0.005	0.007	0.009	0.007	0.009	0.005	0.005	0.005	0.007	0.002	0.004	-	-
Li	0.078	0.102	0.102	0.090	0.125	0.125	0.114	0.114	0.114	0.136	0.000	0.158	0.190	0.940	0.51
Catsum	29.869	29.874	29.885	29.888	29.871	29.837	29.917	29.918	29.844	29.776	29.690	29.815	29.801	29.691	29.33
H	(3)	(3)	(3)	(3)	(3)	(3)	(3)	(3)	(3)	(3)	(3)	(3)	(3)	(4)	(4)

[§] analyses from C. Chopin (pers. comm., 1991)

TABLE 7. COMPARISON OF RESULTS OF ELECTRON-MICROPROBE ANALYSES OF STAUROLITE SAMPLES IN THIS STUDY (TS) AND HOLDAWAY *et al.* (1986b) (HDS)

	71-62R		EH-6		3-3		106038		117189		6-3	
	TS	HDS	TS	HDS	TS	HDS	TS	HDS	TS	HDS	TS	HDS
SiO ₂ wt%	27.74	27.79	27.78	27.13	27.15	27.22	26.62	26.90	27.17	27.46	28.28	28.36
Al ₂ O ₃	54.96	54.95	53.23	53.03	53.91	54.14	54.70	54.56	52.86	52.94	55.18	55.04
TiO ₂	0.36	0.43	0.38	0.47	0.41	0.54	0.30	0.38	0.46	0.53	0.44	0.40
Cr ₂ O ₃	0.02	0.05	0.04	0.06	0.04	0.09	0.01	0.05	0.03	0.06	0.06	0.10
CoO	0.02	0.03	0.04	0.03	0.02	0.02	0.02	0.02	0.02	0.02	0.03	0.02
FeO	12.71	12.83	12.79	12.79	13.99	14.06	10.46	10.37	9.39	9.13	10.99	10.88
MgO	0.65	0.69	3.99	4.02	1.77	1.89	2.61	2.63	1.81	1.93	0.89	0.91
MnO	0.22	0.23	0.14	0.11	0.47	0.48	0.35	0.36	0.12	0.15	0.48	0.43
ZnO	0.17	0.24	0.28	0.30	0.21	0.18	3.12	3.05	6.49	6.33	*0.48	0.99
Li ₂ O	0.36	0.29	0.01	0.01	0.11	-	0.01	0.01	0.05	0.05	0.98	**0.99
H ₂ O	(2.26)	2.26	(1.52)	1.52	(1.43)	1.43	(1.62)	1.62	(1.65)	1.65	(1.80)	1.80
Sum	99.47	99.85	100.20	99.51	99.51	100.10	99.82	99.99	100.05	100.32	99.61	99.92

* this sample is very inhomogeneous (Holdaway, pers. comm., 1992), and this difference in ZnO contents may well reflect this inhomogeneity;

** Holdaway (pers. comm., 1991).

TABLE B. CALCULATION OF VACANCIES AT T(2) IN S(1) FOR UNCOUPLED (u) AND COUPLED (c) M(4) OCCUPANCIES

M(4A)	0.138 Fe ²⁺
M(4B)	0.075 Fe ²⁺
¹ □(u)	0.214(0.85)
¹ □(c)	0.138(0.55)
T(2) site-population (apfu)	
Fe	2.30
Zn	0.03
Mg	0.16
Al	0.31
Li	0.40
□	0.80
Sum	4.00

value in parantheses is per formula unit

powers together; thus Al* = Al (Z = 13) + Mg (Z = 12), and Fe* = Fe²⁺ (Z = 26) + Fe³⁺ (Z = 26) + other transition metals (commonly Ti, Cr, Co, Mn). The assignment of species within these groups must rely on crystal-chemical analysis rather than site-scattering refinement. The situation is further complicated by the fact that some of the sites in the staurolite structure

can also accommodate vacancies. In such cases as this, assignment of site populations has to rely on crystal-chemical argument as well as site-scattering refinement. The problem with such arguments is that they are usually difficult to test. The situation is completely different where a large amount of crystallographic data is available. Then the argument is forced to work for a much larger data set, and one expects to develop quantitative crystal-chemical correlations as a function of mineral composition. Consequently, we will examine each site (or selected pairs of sites) in the staurolite structure, and attempt to derive consistent site-populations. Ionic radii (*r*) are taken from Shannon (1976).

THE T(1) SITE

The site scattering shows that no transition metals occur at this site. Details of the stereochemistry of this site across the range of staurolite crystals are shown in Table 4. The $\langle T(1)-O \rangle$ bond-lengths vary between 1.637 and 1.644 Å, with a mean value of 1.641 Å and a root-mean-square deviation of 0.001 Å. Although this is an extremely restricted range of variation, the electron-microprobe data (Table 6) indicate that there is significant variation in the ²⁷Al content of the T(1) site, from 0.030 to 0.576 apfu. As ²⁸Si (*r* = 0.26 Å) and ²⁷Al (*r* = 0.39 Å) differ significantly in size, there should be a positive correlation between the ²⁷Al content derived from the unit formula (= 8 - Si) and the

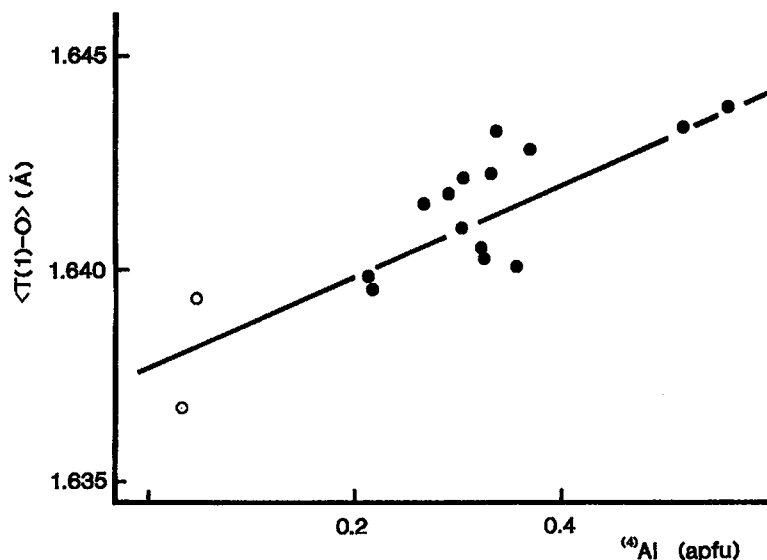


FIG. 6. The variation in $\langle T(1)-O \rangle$ as a function of constituent site-populations (expressed as ²⁷Al) for the fully analyzed staurolite crystals refined in this study (filled circles) and the silica-rich staurolite crystals S(41) and S(42) (hollow circles); the line through the data is not a least-squares line, but is drawn as a guide to the eye.

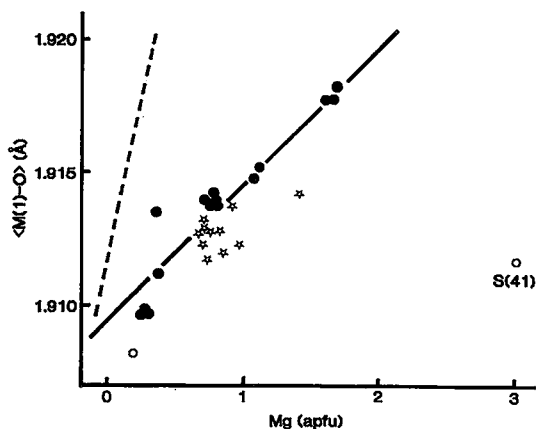


FIG. 7. The variation in $\langle M(1)-O \rangle$ as a function of total Mg content of staurolite; solid circles represent staurolite samples for which complete analyses (*i.e.*, including H_2O) were done, stars represent staurolite samples without H_2O determinations, and hollow circles denote S(41) and S(42). The straight line is the regression line for the solid circles only; the dashed line represents a hard-sphere model for $Al \rightleftharpoons Mg$ replacement.

$\langle T(1)-O \rangle$ distance. As indicated in Figure 6, there is a significant correlation, but because the range of the substitution is small, the correlation is not useful as a predictive indicator of the Al content of the $T(1)$ site. The observed variations in $\langle T(1)-O \rangle$ and ^{14}Al content are compatible with a hard-sphere model, given the size (~ 0.001 Å) of the standard deviations of the $\langle T(1)-O \rangle$ distances, and preclude the possibility of any Mg occurring at $T(1)$.

THE $M(1A)$ AND $M(1B)$ SITES

As these two sites are equivalent in the orthorhombic structure, initially they will be dealt with together and designated as the $M(1)$ site. There are two principal questions here: first, what are the *mean* site-populations (*i.e.*, what is the average compositions of these sites), and secondly, is there any ordering over the two sites?

$M(1)$ site-populations

Unconstrained site-scattering refinement (using Al and Fe scattering factors) shows that this site is dominated by cations with atomic number close to 13 (Table 5). The grand mean site-scattering is 105.04 epfu, indicating a small amount of substitution of transition metals at these two sites; this point will be examined in greater detail later on. Presuming that ^{16}Si is not generally present in staurolite, this leaves

Al and Mg as principal possible constituents of the $M(1A)$ and $M(1B)$ sites. There are eight of these sites in the unit cell, and the composition of staurolite indicates that the constituent cations must be dominated by Al. This is confirmed by the mean bond-lengths of the relevant coordination polyhedra: the grand $\langle M(1)-O \rangle$ distance is 1.913 Å with a root-mean-square deviation of 0.001 Å, within the range expected for an AlO_6 octahedron. Of course, this does not negate the possibility of small amounts of Mg occurring at these sites, and this possibility is examined next.

Figure 7 shows the variation in $\langle M(1)-O \rangle$ as a function of Mg apfu for the staurolite crystals examined in this study. There is a well-developed positive linear correlation, with one very significant outlier at high Mg values. In the range 0–2.0 Mg apfu, there is an increase in $\langle M(1)-O \rangle$; at low Mg values, the Li–Zn-rich S(42) crystal lies significantly below the general trend. The value at 3.01 Mg apfu [S(41)] lies far from the observed trend, and as will be shown later, exhibits completely different behavior with respect to Mg.

There is an interesting compositional observation to make here. The grand $\langle M(1)-O \rangle$ value is 1.913 Å; this corresponds to an Mg content of 0.78 Mg apfu according to the correlation observed. This should be close to the mean Mg content of staurolite, and this is in fact the case. Griffen *et al.* (1982) gave the range of Mg values for 82 samples of staurolite as 0–1.44 apfu; the average value is 0.72 Mg apfu, close to the value of 0.78 Mg apfu for the data of Table 6.

Thus the stereochemical data do indicate that *some* Mg occurs at the $M(1A)$ and $M(1B)$ sites. The next question is “how much?”, as the trend of Figure 7 and the outlier of Mg-rich staurolite S(41) indicate that not all Mg can occur at these sites. We can get a very good idea of the Mg content of the $M(1)$ sites from the behavior of the mean bond-lengths. The ionic radii of ^{16}Al ($r = 0.535$ Å) and ^{16}Mg ($r = 0.72$ Å) are significantly different, and the mean bond-lengths should be a very sensitive indicator of the relative Al–Mg occupancy. The steep line drawn in Figure 7 shows the expected variation in mean bond-length (for a hard-sphere model) if all the Mg in the formula unit were to occupy the $M(1)$ sites; the ideal slope of this line is $(0.72 - 0.535)/8 = 0.023$ (Å per Mg apfu). The slope of the observed trend is 0.0053, 23% of the ideal slope for complete substitution. This slope suggests that over this range, $\sim 23\%$ of the Mg in the formula unit is ordered at the $M(1)$ sites. As the linearity of Figure 7 persists essentially down to zero Mg content, the estimation of 23% Mg content at $M(1)$ can be taken as an absolute content. A different substitution obviously holds for the Mg-rich staurolite S(41). However, this inference is not particularly surprising, as this specific sample of staurolite formed under conditions of unusually high pressure.

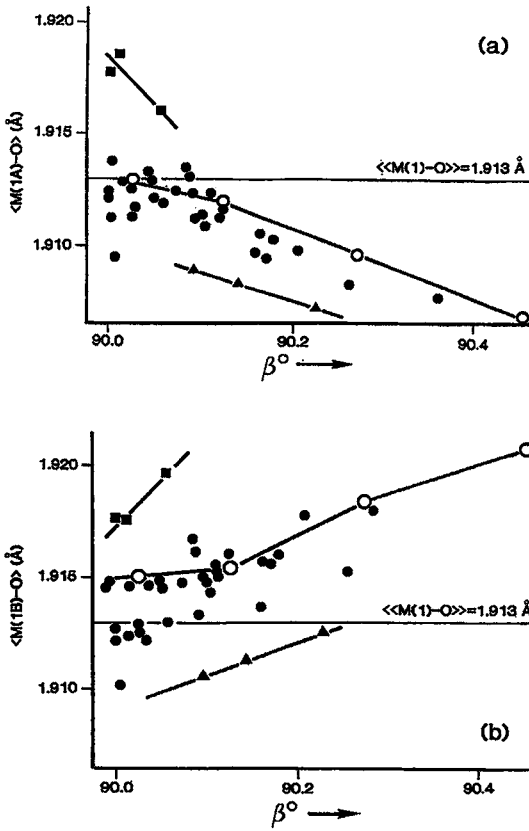


FIG. 8. The variation in $\langle M(1A)-O \rangle$ (a) and $\langle M(1B)-O \rangle$ (b) as a function of β angle in all the staurolite crystals refined here. Solid lines show variation within single samples; solid triangles: S(1–3), sample 71–62R; solid squares: S(4–6), sample EH–6; hollow circles: S(11–14), sample 117189.

Any substitution of Fe^{3+} , Ti^{4+} and Cr^{3+} at $M(1)$ could change the estimate of the Mg content, as these transition metal cations also are larger than Al. The total range of variation in Al–Fe occupancy as derived from the site-scattering values of Table 5 is 0.000–0.027 Fe^{3+} . A substitution to this extent is expected to affect the mean bond-length by $0.027 \times (0.645 - 0.535) = 0.003 \text{ \AA}$. This difference is substantial with regard to the changes we are observing, but will only be of significance if the substitution is correlated in some fashion with Mg site-populations. As there is no correlation between the refined site-scattering from $M(1)$ and the Mg content, any transition-metal content of $M(1)$ is not contributing systematically to the variation in mean bond-length shown in Figure 7.

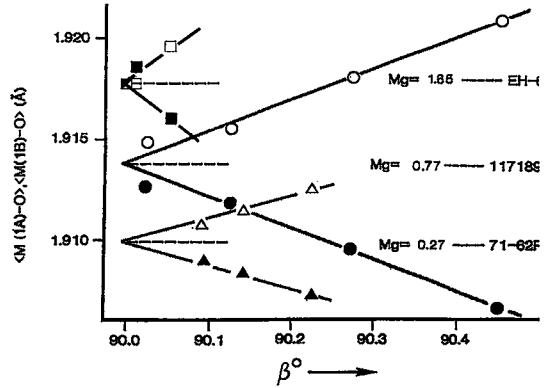


FIG. 9. The variation in $\langle M(1A)-O \rangle$ (full symbols) and $\langle M(1B)-O \rangle$ (hollow symbols) as a function of β angle for selected crystals of staurolite with different Mg contents.

$M(1A)-M(1B)$ ordering

Given that small amounts of Mg occur at the $M(1)$ sites, the question now arises as to whether or not there is any preferential ordering of Mg over the $M(1A)$ and $M(1B)$ sites. Again, we must evaluate this possibility using variations in mean bond-length because of the insensitivity of X-ray scattering to Al–Mg ordering. However, we must also allow for the fact that variations in the mean bond-lengths of the $M(1A)$ and $M(1B)$ octahedra may be induced by changes in Al – \square order over the $M(3A)$ and $M(3B)$ sites. This possibility is examined in Figure 8, which shows the variations in $\langle M(1A)-O \rangle$ and $\langle M(1B)-O \rangle$ as a function of β . With increasing β , $\langle M(1A)-O \rangle$ decreases and $\langle M(1B)-O \rangle$ increases, such that $\langle M(1)-O \rangle$ remains approximately constant (except for the compositional trend of Fig. 7). First, the data indicate that at $\beta = 90^\circ$, $\langle M(1A)-O \rangle \approx \langle M(1B)-O \rangle \approx 1.910\text{--}1.918 \text{ \AA}$. Second, the data for the Zn-rich staurolite 117189 [crystals S(11), S(12), S(13) and S(14)] span the complete range of data; as these crystals all have the same bulk composition, the general trend of the data must be controlled not by compositional variations but by the degree of order associated with the Al – \square ordering over $M(3A)$ and $M(3B)$. The intercepts of the trends for S(1)–S(3) and S(4)–S(6) (Fig. 8) show the expected range in $\langle M(1)-O \rangle$ as a function of chemical composition at $M(1)$. This behavior is further illustrated by the data for 71–62R, 117189 and EH–6 in Figure 9. Here it can be seen that the actual divergence of the sizes of the $M(1A)$ and $M(1B)$ octahedra as a function of β occurs for all values of Mg content, with only the $\langle M(1)-O \rangle$ value affected by the Mg content. Examination of Figure 9 suggests that the relative divergence of the sizes of the $M(1A)$ and $M(1B)$ octahedra as a function of β increases with increasing

Mg content of the staurolite. The slope (in \AA°) of the lines increases as a function of Mg content, from 0.009 for 71–62R (0.27 Mg apfu) to 0.0155 for 117189 (0.77 Mg apfu) to 0.030 for EH-6 (1.65 Mg apfu); because of the scatter in the data, as well as the restricted range of β shown by the EH-6 crystals, we do not consider this point to be well established. However, it does suggest a different response of $M(1A)$ and $M(1B)$ to increasing β with differing Mg content. There are two possibilities here:

(i) Mg is always totally disordered over $M(1A)$ and $M(1B)$, and the different response to changing β for different Mg contents reflects the greater susceptibility of $M(1A)$ and $M(1B)$ octahedra with lower aggregate charge (*i.e.*, higher Mg content) to inductive effects from the rest of the structure, specifically Al–□ ordering over $M(3A)$ and $M(3B)$.

(ii) Mg is disordered over $M(1A)$ and $M(1B)$ for $\beta = 90^\circ$, and increasing β correlates with Mg–Al ordering over $M(1A)$ and $M(1B)$. In this way, the different response to Al–□ disorder for differing Mg contents reflects the increased Mg content at $M(1B)$ relative to that at $M(1A)$ with increased total Mg in the crystal.

At the moment, we have no way of distinguishing these two possibilities because of the low Mg content at the $M(1)$ site; however, it is definitely established that some Mg occupies the $M(1A)$ or $M(1B)$ sites (or both).

THE $M(2)$ SITE

The observed mean bond-lengths (Table 4) and the site-scattering refinements (Table 5) show this site to be dominated by Al. The question now is whether or not there is significant occupancy by Mg or transition metals such as Fe^{3+} , Ti^{4+} and Cr^{3+} .

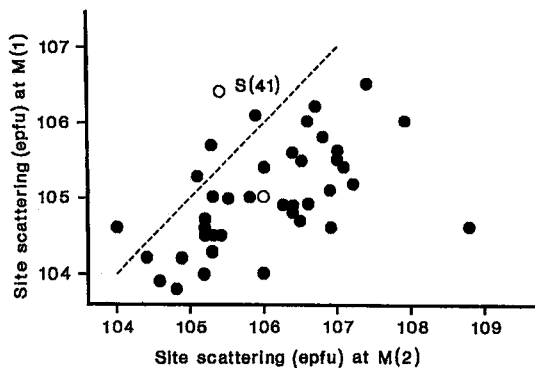


FIG. 10. Comparison of the refined scattering at the $M(1)$ and $M(2)$ sites in staurolite crystals. The dashed line corresponds to identical scattering from $M(1)$ and $M(2)$, hollow circles are S(41) and S(42).

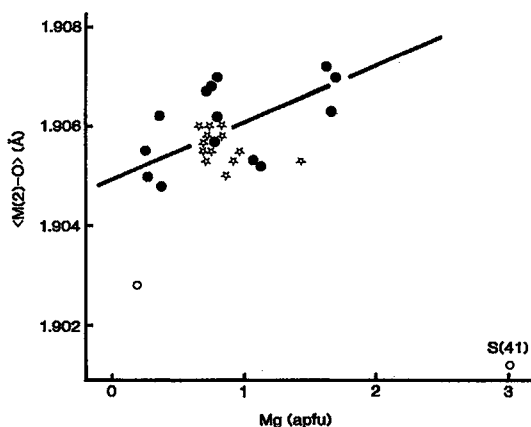


FIG. 11. The variation in $\langle M(2)-O \rangle$ as a function of total Mg content of staurolite; legend as in Figure 7.

The site-scattering is slightly in excess of 104 epfu (*i.e.*, $8 \times 13 e$), indicating very minor occupancy of $M(2)$ by transition metals of some sort; note that the same result was obtained for the $M(1)$ sites. The relative behavior of the refined site-scattering at $M(1)$ and $M(2)$ is examined in Figure 10. The diagonal line in this figure indicates complete disorder of any transition metals over $M(1)$ and $M(2)$. Most of the data occur to the right of the “disorder” line, indicating that any transition metals that occur at these two (sets of) sites are preferentially (but not completely) ordered at the $M(2)$ site.

The dispersion of $\langle M(2)-O \rangle$ distances in all crystals refined (Table 4) is extremely limited. The grand $\langle M(2)-O \rangle$ distance is 1.906 \AA , with a root-mean-square deviation of 0.001 \AA , and the individual mean bond-lengths vary 0.002 \AA across the total range of composition. There is no correlation between $\langle M(2)-O \rangle$ and the $M(2)$ site-scattering or the β angle. Figure 11 shows the variation in $\langle M(2)-O \rangle$ as a function of total Mg content of the crystal. There is a weak linear correlation, again with staurolite S(41) as an outlier. The slope of the correlation is 0.0013, as compared with the ideal slope of 0.023 for complete substitution of Mg for Al. This indicates that 6% of the Mg substitutes at $M(2)$, and the site populations were so assigned.

Thus the variations in refined site-scattering and mean bond-lengths are compatible with only very minor incorporation of components other than Al at the $M(2)$ site.

THE $M(3A)$ AND $M(3B)$ SITES

The Al – □ ordering over the $M(3A)$ and $M(3B)$ sites is a feature of major importance in the staurolite

structure. With regard to site populations, there are three principal problems:

- (i) is the total cation content of the $M(3)$ sites fixed or variable?
- (ii) is there significant substitution of other species at $M(3)$ (e.g., Mg, Fe^{3+} , etc.) in addition to Al and \square ?
- (iii) if there are other cations at $M(3)$ in addition to Al, do they show different patterns of order over $M(3A)$ and $M(3B)$?

$M(3)$ site-populations: cations versus vacancies

The site-scattering values of the $M(3A)$ and $M(3B)$ sites are given in Table 5. The grand mean site-scattering of $M(3A)$ and $M(3B)$ for the 42 crystals refined here is 25.74 epfu ($\equiv \text{Al}_{1.98} + \square_{2.02}$ pfu) with a root-mean-square deviation of 0.76. Thus there is a small but significant variation in the aggregate scattering from the $M(3)$ sites, with a total range of 23.58–27.06 epfu. Much of this variation is due to the H-rich staurolite crystals, which show low aggregate $M(3)$ scattering (mean value = 23.78 epfu). Omitting these crystals [S(1–3), S(42)], the mean $M(3)$ scattering for the remaining crystals is 25.94 epfu; nevertheless, there is still a significant range in $M(3)$ scattering (25.12–27.06 epfu).

We need to consider three possible types of substitution at these sites: $\text{Fe}^* \rightleftharpoons \text{Al}$, $\text{Mg} \rightleftharpoons \text{Al}$ and $\text{Li} \rightleftharpoons \text{Al}$. Only the first and third types of substitution significantly affect the scattering power at the $M(3)$ sites, and so we will consider these substitutions first. The $\text{Fe}^{3+} \rightleftharpoons \text{Al}$ substitution will increase the effective scattering as Fe (26) scatters X rays more strongly than Al^* (13); the second substitution will decrease the effective scattering as Li (3) scatters X rays less strongly than Al^* (13). The basic situation may thus be summarized as follows [treating $M(3A)$ and $M(3B)$ as summed for the moment]: there are four scattering species, Al^* ($\equiv \text{Al} + \text{Mg}$), Fe^* ($\equiv \text{Fe}, \text{Ti}, \text{Cr}, \text{Zn}, \text{Co}$), Li and \square to be assigned to one site. There is no unique solution to this problem if only the site-scattering values are considered.

The first question to resolve is whether the Al^* content of the $M(3)$ sites is always exactly 2.0 apfu, with the range of refined scattering resulting from substitution of other species (i.e., Li, Fe) for Al at these sites. In this case, site-scattering less than 26 epfu could only be caused by substitution of atoms with lower scattering power than Al (13); the only possible cation of significance here is Li, which Dutrow *et al.* (1986) have shown to be a significant component in some staurolite samples. The H-rich staurolite always seems to have significant Li content, sufficient to account for the low refined scattering at their $M(3)$ site(s). This is a tempting hypothesis, as it would account for the presence of significant Li in *all* the H-rich staurolite samples analyzed (77–55C, 71–60E, 71–62R from Holdaway *et al.* 1986b; S(41) from Chopin, pers.

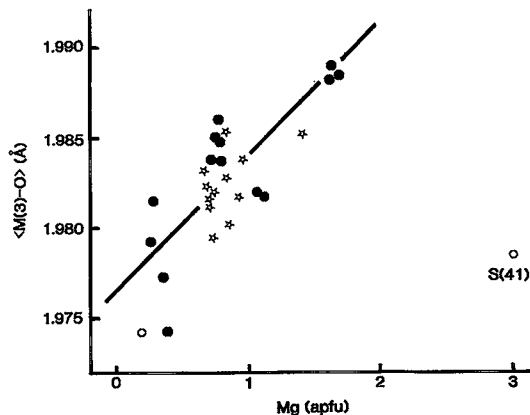


FIG. 12. The variation in $\langle M(3)\text{-O} \rangle$ as a function of total Mg content of staurolite; legend as in Figure 7.

comm.). However, if such a substitution occurs, it should significantly affect the $\langle M(3)\text{-O} \rangle$ distance, as ^{6}Li ($r = 0.535 \text{ \AA}$) is a lot smaller than ^{6}Al ($r = 0.76 \text{ \AA}$). As an example, for crystal S(1), the Li content of $M(3)$ would need to be 0.23 apfu; this would increase the $\langle M(3)\text{-O} \rangle$ distance by $\sim 0.008 \text{ \AA}$ (when taking into account changes in the proportion of vacancies). Inspection of Table 4 shows that $\langle M(3)\text{-O} \rangle$ for S(1) (and all the other crystals of H-rich staurolite) is in the same range as all the other staurolite crystals with $M(3)$ scattering close to 26 epfu. This indicates that there is insignificant Li at $M(3)$ in the H-rich staurolite. Thus the low refined scattering from $M(3)$ in the H-rich staurolite crystals *must* be caused by additional vacancies at $M(3)$.

Now we need to consider the possibility of significant Fe^* substitution at $M(3)$. The maximum refined scattering at $M(3)$ is for crystal S(5); assuming exact half-occupancy of $M(3)$, the refined scattering corresponds to an $M(3)$ content of $[0.08 \text{ Fe}^* + 1.92 \text{ Al} (+ \text{Mg}) + 2.00 \square]$. If Fe^* is Fe^{3+} (or Cr^{3+} or Ti^{4+}), the site population would lead to an increase of 0.005 \AA over zero Fe^* occupancy; if Fe^* is Fe^{2+} , the corresponding increase would be 0.006 \AA . Both of these are reasonably consistent with the observed $\langle M(3)\text{-O} \rangle$ distance in crystal S(5). However, as we see in the next section, the variation in $\langle M(3)\text{-O} \rangle$ distance correlates well with the bulk Mg content of the crystal, indicating that the small variations observed in $\langle M(3)\text{-O} \rangle$ are due primarily to variable Mg content (rather than the incorporation of Fe^{2+}). Thus if there is significant Fe^* at $M(3)$, it must be Fe^{3+} (or Cr^{3+} or Ti^{4+}) rather than Fe^{2+} or Mn^{2+} . However, at the moment we have no basis for assigning such populations, as we must conclude from the arguments given above that there is

variable total occupancy of cations at the $M(3)$ site across the range of staurolite compositions.

Mg at $M(3)$

The last point concerning $M(3)$ is whether or not significant amounts of Mg occur at these sites. Figure 12 shows the variation in $\langle M(3)-O \rangle$ as a function of bulk Mg content of the crystal. Omitting the H-rich staurolite crystals for the reasons mentioned above, there is a fairly good linear correlation that can be interpreted as being due to small amounts of Mg occurring at $M(3)$. From the slope of the correlation and the relative sizes of Al and Mg, the Mg content of $M(3)$ is calculated as ~10% of the total Mg apfu; Mg populations were assigned accordingly.

THE $M(4A)$ AND $M(4B)$ SITES

These sites are partially occupied, and are octahedrally coordinated; the octahedra each share one set of opposing faces with adjacent $T(2)$ tetrahedra. It is notable that the $M(4A)-T(2)$ and $M(4B)-T(2)$ distances are both ~1.65 Å, and consequently there must be some sort of local ordering of cations and vacancies, as these distances are too short for simultaneous occupancy of adjacent $M(4)$ and $T(2)$ sites.

The refined scattering from the $M(4A)$ and $M(4B)$ sites is given in Table 5; values range from 0 [completely vacant: S(15), S(16)] to 12.4 epfu [S(41), the Mg-rich staurolite of Chopin, pers. comm.]. However, the chemical identity of the cations occupying the $M(4)$ sites is rather a difficult problem, primarily because of the very low scattering at these sites. The best chance of getting some idea of the type of cations at $M(4)$ is to consider those samples with high $M(4)$ scattering [S(1-3) and S(41)]. At first, there seems no obvious correlation with bulk composition; samples 71-62R [crystals S(1-3)] and S(41) show few (if any) common compositional characteristics (Table 6). However, one can get some clue by comparing 71-62R, in which there is a large $M(4)$ scattering, with 6-3, in which the $M(4)$ scattering is zero. In a solid solution, the size of the polyhedron coordinating the cation(s) changes in response to the different radii of the constituent cations; this observation is the case in both cation \rightleftharpoons cation substitutions and in $\square \rightleftharpoons$ cation substitutions, provided we realize that the radius of the vacancy is a function of the structure in which it occurs. We may regard the $M(4)$ sites as participating in a cation \rightleftharpoons \square substitution; in the present case, staurolite 6-3 is the vacancy end-member, and staurolite 71-62R is an intermediate member with partial occupancy of the $M(4)$ sites. However, both of these have identical $\langle M(4)-O \rangle$ distances of 2.162 Å. This indicates that we are substituting a cation at the $M(4)$ site that is the same size as the vacancy at the $M(4)$ site, and thus we can calculate the (mean) radius of the sub-

stituent cation(s) at $M(4)$ by subtracting the radius of oxygen from the observed mean bond-length. Taking $r(\text{oxygen}) = 1.38$ Å, $r_{\text{cat}} = 2.16 - 1.38 = 0.78$ Å, which is the ionic radius of [6]-coordinate Fe^{2+} . This indicates that Fe^{2+} occupies the $M(4)$ sites in staurolite 71-62R.

This rather convoluted reasoning also is supported by stoichiometric arguments involving the $M(4)$ site-populations. The $M(4)$ scattering in staurolite 71-62R is 10.8 epfu, which is equivalent to 0.90 Mg or 0.42 Fe apfu. As discussed later, each occupied $M(4)$ site is accompanied by 2 \square at adjacent $T(2)$ sites. If the $M(4)$ site-populations were 0.90 Mg apfu, this would mean at least 1.80 \square pfu and a maximum of 2.2 apfu of any kind at the $T(2)$ site. This is not consistent with the observed scattering at the $T(2)$ site, which indicates a minimum content of $\sim 0.68 \times 4 = 2.72$ Fe apfu; thus Mg does not occur at the $M(4)$ sites in staurolite 71-62R. Also, staurolite 71-62R only has 0.284 Mg apfu [of which we have already assigned half to the $M(1,2,3)$ sites], confirming our stereochemical arguments. With 0.42 Fe^{2+} apfu at $M(4)$, this indicates 0.86 \square at the $T(2)$ site, a value that is compatible with the observed scattering. As we will see later, $M(4A)$ and $M(4B)$ are usually occupied by Fe^{2+} . However, in specific cases of unusual composition or conditions of formation [e.g., high-pressure Mg-rich staurolite S(41)], Mg may also occupy $M(4A)$ and $M(4B)$.

LOCAL CATION - \square ORDERING AT $T(2)$ AND $M(4)$

A crucial part of assigning site populations at the $T(2)$ site is the assessment of the vacancy content, and consequently this must be considered before the $T(2)$ site-populations can be reliably assigned. The $M(4A)$ and $M(4B)$ octahedra share faces with the $T(2)$ tetrahedron, and the corresponding site-separations are extremely short: $M(4A)-T(2) \approx M(4B)-T(2) \approx 1.65$ Å. Consequently, sites that are locally adjacent across a shared polyhedral face cannot be simultaneously occupied by cations, even if the effects of local relaxation associated with $T(2)$ positional disorder are considered; thus local (short-range) ordering of cations and vacancies must occur. Such models of local order are easy to construct but usually difficult to confirm experimentally. However, in the present case, some of the more extreme compositions provide a sufficient test of these models.

Locally uncoupled $M(4A)$ and $M(4B)$ occupancy

Here it is assumed that occupancy of a specific $M(4A)$ site is unrelated to the occupancy of the adjacent $M(4B)$ sites [i.e., there is complete local disorder of the $M(4)$ occupancies]. Each occupied $M(4A)$ site forces vacancies at the two adjacent $T(2)$ sites; similarly, each occupied $M(4B)$ site forces vacancies at the

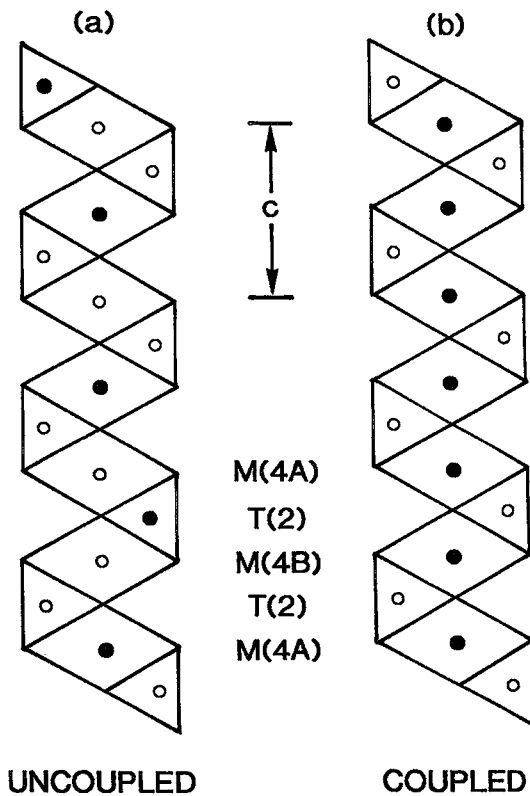


FIG. 13. Models for uncoupled and coupled occupancy of the $M(4)$ and $T(2)$ polyhedra: (a) uncoupled occupancy of $M(4A)$ and $M(4B)$; occupancy of an $M(4A)$ site is not coupled to the occupancy of an adjacent $M(4B)$ site; (b) coupled occupancy of $M(4A)$ and $M(4B)$; occupancy of an $M(4A)$ site is coupled to occupancy of an adjacent $M(4B)$ site; a totally ordered situation is shown here, although disordered configurations [with lower aggregate $M(4)$ occupancies] are usually the case.

two adjacent $T(2)$ sites (Fig. 13a). The total number of vacancies at the $T(2)$ site is thus $[2 M(4A) + 2 M(4B)]$ pfu.

Locally coupled $M(4A)$ and $M(4B)$ occupancy

Here it is assumed that occupancy of a specific $M(4A)$ site is coupled to the occupancy of the adjacent $M(4B)$ sites (*i.e.*, there is maximum local order). This results in an edge-sharing chain of occupied $M(4A)$ and $M(4B)$ octahedra (Fig. 13b). Within this chain, each occupied $M(4A)$ site forces vacancies at the two adjacent $T(2)$ sites, as before. However, the associated

occupied $M(4B)$ sites do not have a similar effect, as their locally associated $T(2)$ sites are already vacant. As the occupancy of $M(4A)$ is always greater than the occupancy of $M(4B)$, the total number of $T(2)$ site vacancies is $2 [M(4A)]$ pfu.

Testing the models

These two models can be regarded as extremum models representing total $M(4A)$ – $M(4B)$ local disorder and total $M(4A)$ – $M(4B)$ local order, respectively, with associated populations of vacancies at the $T(2)$ site of $2 [M(4A) + M(4B)]$ and $2 [M(4A)]$, respectively. For those crystals of staurolite in which the (cation) site populations of the $M(4)$ sites are considerable, these two models have significantly different compositional implications, differences that may be sufficient to distinguish between the two “end-member” models. There are two ways in which we may test these models:

- (i) to consider the effect of the resulting $M(4)$ site-populations on the vacancy populations of $T(2)$;
- (ii) to consider the effects of $M(4A)$ – $M(4B)$ ordering on $T(2)$ site-populations with varying β angle.

$M(4)$ occupancy and $T(2)$ vacancies: consider first staurolite 71–62R [crystals S(1), S(2) and S(3)]. This sample has a large $M(4)$ site-scattering of ~ 10.7 electrons that we have previously shown to be due to Fe^{2+} . The details of the vacancy calculation are shown in Table 8. The amounts of $T(2)$ vacancies from the uncoupled and coupled models are 0.85 and 0.55 \square pfu, respectively. Comparison with the site-populations assigned to the $T(2)$ site shows the *uncoupled model to agree with the assigned site-populations*. Thus the arguments of this section indicate that the uncoupled model for $M(4)$ site occupancy gives the correct proportion of vacancies at the $T(2)$ site. For most of the other samples, the $M(4)$ site-populations are not sufficiently large for the differences in the calculated vacancies to be significant.

$M(4A)$ – $M(4B)$ ordering and $T(2)$ occupancy: now we consider the effect of varying $M(4A)$ – $M(4B)$ order on the site population of $T(2)$ with varying β for crystals of the same composition. By far the most important samples in this regard are staurolite 117189 and 71–62R, both of which show significant ranges of β for the different crystals examined. The key argument here is this: if the $M(4)$ occupancies are locally uncoupled, the $T(2)$ vacancies are $2 [M(4A) + M(4B)]$ pfu, which is independent of the degree of $M(4A)$ – $M(4B)$ order; if the $M(4)$ occupancies are locally coupled, the $T(2)$ vacancies are $2 [M(4A)]$ pfu, and thus will vary with the degree of $M(4A)$ – $M(4B)$ order as a function of β . These models are examined graphically for staurolite 117189 [crystals S(11–14)] and 71–62R [crystals S(1–3)] in Figure 14. The lowest β value for each sample is taken as the “starting value”, and the changes in $T(2)$ populations are examined as a func-

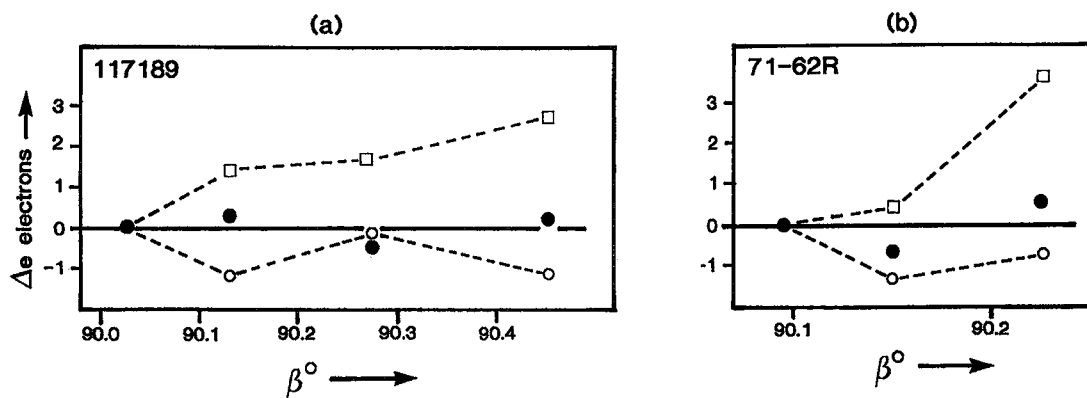


FIG. 14. Variation in $T(2)$ site-scattering (expressed in electrons pfu) as a function of β angle for staurolite samples (a) 117189, and (b) 71-62R; the observed data (full circles) and the ideal variation for both coupled (hollow squares) and uncoupled (hollow circles) occupancy of $M(4A)$ and $M(4B)$ are shown.

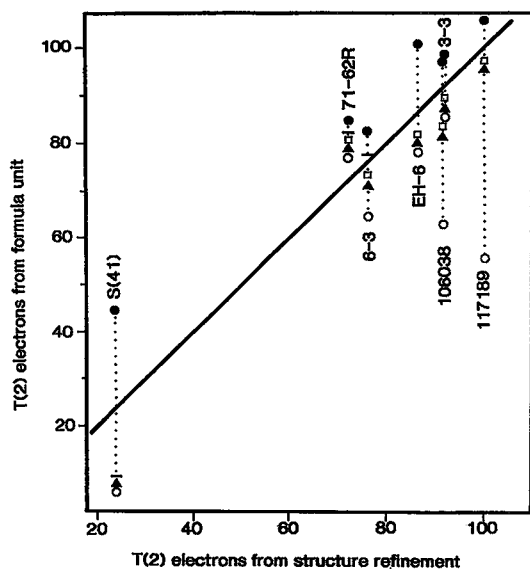


FIG. 15. The total number of electrons at the $T(2)$ site from the site-scattering refinement and from the available cations as indicated by the results of the electron- and ion-microprobe analyses; only selected samples are shown for clarity. Symbols denote electrons available from specific combinations of cations; hollow circles: [Fe]; triangles: [Fe + Zn]; hollow squares: [Fe + Zn + M^{n+} (Mn + Ti + Cr + Co)]; horizontal line: [Fe + Zn + M^{n+} + Li]; full circles: [Fe + Zn + M^{n+} + Li + Mg]. Where specific symbols are missing, they overlap symbols already present [*i.e.*, the additional cation contributes few electrons to the possible $T(2)$ scattering]. The diagonal line indicates 1:1 correspondence between the number of electrons from the structure refinement and the electrons from the formula unit. Hence one can read from this diagram which cations *must* occur at $T(2)$.

tion of β . For the uncoupled model, the site-population of $T(2)$ should stay unchanged; for the coupled model, it should increase with increasing β as the degree of $M(4A)$ – $M(4B)$ order becomes more pronounced. For staurolite 117189, the observed $T(2)$ scattering values (in epfu) favor the uncoupled model; the values for staurolite 71-62R are perhaps intermediate between the two models, but are still closer to the uncoupled model.

Thus the arguments of the last two paragraphs support the locally uncoupled model. As will be shown later, the reason for the Fe^{2+} disorder between $T(2)$ and $M(4)$ is connected with the fact that occupancy of the $M(4A)$ and $M(4B)$ sites is locally uncoupled.

$T(2)$ SITE

The results of the site-scattering refinements are given in Table 5. There is no unique way of assigning specific chemical site-populations to $T(2)$ simply from the diffraction results, and consequently we must use a combination of the diffraction results, electron- and ion-microprobe results, and stereochemical evidence.

Some qualitative considerations

As a first step, we need to compare the numbers of electrons known to be present at the $T(2)$ site from the refinement results with the numbers of electrons available from each different cation [usually considered as occupying the $T(2)$ site], as indicated from the electron- and ion-microprobe results. This is done in Figure 15; not all crystals are shown or the detail would be obscured, but a range of chemical types is represented. The obvious conclusions from Figure 15

TABLE 9. SITE-POPULATIONS IN STAUROLITE CRYSTALS

	S(1)	S(2)	S(3)	S(4)	S(5)	S(6)	S(7)	S(8)	S(9)	S(10)	S(12)	S(13)	S(15)	S(16)	S(17)	S(18)
M(1) Al	7.81	7.85	7.84	7.43	7.47	7.49	7.70	7.75	7.73	7.73	7.69	7.67	7.79	7.70	7.54	7.71
Mg	0.07	0.07	0.06	0.39	0.45	0.40	0.19	0.17	0.27	0.26	0.26	0.26	0.09	0.09	0.34	0.17
Fe*	0.12	0.08	0.10	0.18	0.08	0.11	0.11	0.10	0.00	0.01	0.05	0.07	0.12	0.21	0.12	0.12
M(2) Al	7.79	7.84	7.89	7.68	7.75	7.74	7.81	7.85	7.77	7.87	7.78	7.75	7.80	7.76	7.68	7.85
Mg	0.02	0.02	0.02	0.11	0.15	0.11	0.05	0.05	0.07	0.07	0.12	0.16	0.02	0.02	0.09	0.05
Fe*	0.19	0.14	0.09	0.21	0.10	0.15	0.14	0.11	0.16	0.06	0.10	0.09	0.18	0.22	0.23	0.10
M(3) Al	1.77	1.66	1.67	1.80	1.88	1.79	1.97	1.97	1.87	1.90	1.89	1.88	1.87	1.98	1.80	1.93
Mg	0.03	0.03	0.03	0.20	0.20	0.20	0.09	0.09	0.13	0.13	0.07	0.08	0.04	0.04	0.17	0.08
Fe*	0.01	0.07	0.09	0.03	0.01	0.04	0.00	0.04	0.01	0.00	0.00	0.02	0.03	0.00	0.03	-
[]	2.19	2.24	2.21	1.97	1.91	1.97	1.94	1.90	1.99	1.97	2.04	2.02	2.06	1.98	2.00	1.99
M(4) Fe*	0.43	0.40	0.41	0.12	0.11	0.11	0.09	0.10	0.13	0.14	0.10	0.09	0.00	0.00	0.19	0.14
[]	3.57	3.60	3.59	3.88	3.89	3.89	3.91	3.90	3.87	3.86	3.90	3.91	4.00	4.00	3.81	3.86
T(1) Si	7.65	7.68	7.69	7.73	7.67	7.71	7.67	7.64	7.48	7.44	7.68	7.70	7.78	7.78	7.66	7.42
Al	0.35	0.32	0.31	0.27	0.33	0.29	0.33	0.36	0.52	0.56	0.32	0.30	0.22	0.22	0.34	0.58
T(2) Fe*	2.37	2.35	2.39	2.56	2.78	2.69	3.15	3.20	2.28	2.42	2.12	2.07	2.42	2.32	2.30	3.18
Zn	0.03	0.04	0.04	0.06	0.06	0.05	0.04	0.04	0.64	0.65	1.33	1.40	0.11	0.09	0.03	0.03
Mg	0.16	0.15	0.15	0.92	0.88	0.94	0.45	0.40	0.64	0.61	0.31	0.29	0.21	0.22	0.82	0.40
Li	0.40	0.40	0.40	0.02	0.01	0.02	0.09	0.16	0.01	0.01	0.06	0.06	1.02	1.15	0.03	0.09
Al	0.19	0.26	0.20	0.20	0.01	0.08	0.09	0.00	0.17	0.04	0.00	0.00	0.24	0.22	0.44	0.02
[]	<u>0.85</u>	<u>0.80</u>	<u>0.82</u>	<u>0.24</u>	<u>0.22</u>	<u>0.22</u>	<u>0.18</u>	<u>0.20</u>	<u>0.26</u>	<u>0.27</u>	<u>0.21</u>	<u>0.18</u>	<u>0.00</u>	<u>0.00</u>	<u>0.38</u>	<u>0.28</u>
Sum T(2)	<u>4.00</u>															
e ^{occ}	68.1	68.7	69.0	82.1	85.3	83.8	90.0	89.7	88.4	90.3	98.5	99.4	75.0	72.0	76.4	89.0
e ^{ref}	71.3	70.6	71.9	86.4	84.9	86.0	92.3	91.3	89.8	90.7	102.6	103.9	78.1	72.6	77.0	90.1

Fe* = Fe²⁺ + Mn + Co + Cr + Ti + Fe³⁺;

e^{occ} = number of electrons at T(2) from assigned site-populations;

e^{ref} = number of electrons at T(2) from site-scattering refinement

are as one would expect. In most cases (*i.e.*, Fe²⁺- and Zn-rich staurolite crystals), the majority of Fe and Zn must be assigned to the T(2) site to account for the observed scattering. However, it is also apparent that if all the Fe and Zn is so assigned, there is still not enough scattering power assigned to T(2). As the refinement results also indicate small amounts of transition metals at octahedrally coordinated sites, it is necessary that other cations (*e.g.*, Mg, Al, Ti, Mn, Li, but not necessarily all of them) occur at T(2). The Mg-rich crystal S(41) also is of interest. It is apparent that the amount of Mg available greatly exceeds the amount of scattering at T(2), and thus much Mg must occur at other sites in the structure; this is in line with our previous assignment of large amounts of Mg to the M(4A) and M(4B) sites in this crystal. It also is apparent for S(41) that the uncoupled model for M(4A) and M(4B) occupancy is not compatible with either the observed stoichiometry or the refined scattering at the T(2) site. Obviously the very high pressure of formation for this particular sample has strongly affected this aspect of its short-range order.

The position of Li in staurolite

The results of the site-scattering refinements and the mean bond-lengths show that significant amounts of Li do not occur at the M(1,2,3) sites. Thus for a cation sum of 30 apfu, there are two "end-member" possibilities for the distribution of Li: (i) Li occurs at T(2), (ii) Li occurs at M(4A) and M(4B) in a coupled arrangement.

Site-scattering refinement of crystals S(15) and S(16) show essentially no electron density at the M(4A) and M(4B) sites. One atom of Li distributed over M(4A) and M(4B) would result in an aggregate M(4) scattering of three electrons, similar to that observed in the Li-poor staurolite crystals; no such electron density is observed in S(15) and S(16). Thus Li must occur at the T(2) site, and the scattering from this site in Li-rich staurolite crystals is in agreement with this.

Vacancies at T(2)

There are four T(2) sites pfu. However, it is com-

TABLE 9. CONTINUED.

	S(20)	S(22)	S(23)	S(24)	S(25)	S(26)	S(27)	S(30)	S(33)	S(35)	S(36)	S(39)	S(40)	S(41)	S(42)
M(1) Al	7.70	7.76	7.70	7.73	7.73	7.66	7.74	7.76	7.70	7.75	7.78	7.79	7.64	7.78	7.95
Mg	0.23	0.24	0.25	0.20	0.20	0.18	0.23	0.23	0.18	0.18	0.16	0.17	0.17	0.14	-
Fe*	0.07	0.00	0.05	0.07	0.07	0.16	0.03	0.01	0.12	0.07	0.06	0.04	0.19	0.08	0.05
M(2) Al	7.94	7.82	7.73	7.84	7.77	7.65	7.85	7.83	7.71	7.75	7.77	7.85	7.69	7.84	7.89
Mg	0.06	0.08	0.05	0.06	0.05	0.05	0.11	0.11	0.05	0.05	0.04	0.05	0.05	0.05	-
Fe*	0.00	0.10	0.22	0.10	0.18	0.30	0.04	0.06	0.24	0.20	0.19	0.10	0.26	0.11	0.11
M(3) Al	1.87	1.89	1.90	1.90	1.94	1.84	1.88	1.90	1.91	1.91	1.64	1.91	1.84	1.98	1.85
Mg	0.12	0.11	0.10	0.10	0.10	0.09	0.12	0.10	0.09	0.09	0.08	0.09	0.08	0.02	-
Fe*	-	-	-	-	-	-	-	-	-	-	0.12	-	0.04	-	-
[]	2.01	2.00	2.00	2.00	1.96	2.07	2.00	2.00	2.00	2.00	2.16	2.00	2.04	2.00	2.15
M(4) Fe*	0.17	0.14	0.13	0.14	0.20	0.24	0.12	0.14	0.19	0.25	0.15	0.19	0.14	1.04*	0.19
[]	3.83	3.86	3.87	3.86	3.80	3.76	3.88	3.86	3.81	3.75	3.85	3.81	3.86	2.96	3.81
T(1) Si	7.51	7.57	7.48	7.48	7.67	7.62	7.53	7.52	7.58	7.58	7.58	7.61	7.74	7.96	7.97
Al	0.49	0.43	0.52	0.52	0.33	0.38	0.47	0.48	0.42	0.42	0.42	0.39	0.26	0.04	0.03
T(2) Fe*	3.00	3.03	2.93	3.03	2.82	2.47	3.39	3.36	2.85	2.59	2.76	2.48	2.73	-	-
Zn	0.06	0.11	0.08	0.08	0.20	0.22	0.03	0.03	0.09	0.10	0.04	0.54	0.04	0.02	2.45
Mg	0.55	0.57	0.42	0.49	0.47	0.43	0.24	0.26	0.41	0.42	0.38	0.42	0.40	1.76	0.19
Li	0.08	0.10	0.10	0.09	0.12	0.12	0.11	0.11	0.11	0.13	0.00	0.16	0.21	0.94	0.51
Al	0.02	0.00	0.22	0.04	0.02	0.42	0.01	0.00	0.17	0.28	0.52	0.03	0.38	-	0.17
[]	<u>0.34</u>	<u>0.28</u>	<u>0.26</u>	<u>0.28</u>	<u>0.40</u>	<u>0.48</u>	<u>0.24</u>	<u>0.28</u>	<u>0.38</u>	<u>0.50</u>	<u>0.30</u>	<u>0.38</u>	<u>0.28</u>	<u>1.28</u>	<u>0.38</u>
Sum T(2)	<u>4.03</u>	<u>4.09</u>	<u>4.01</u>	<u>4.01</u>	<u>4.03</u>	<u>4.16</u>	<u>4.01</u>	<u>4.04</u>	<u>4.01</u>	<u>4.02</u>	<u>4.00</u>	<u>4.01</u>	<u>4.04</u>	<u>4.00</u>	<u>3.70</u>
e ^{occ}	86.9	89.5	86.8	87.9	85.6	82.1	92.5	91.7	84.3	79.5	84.3	86.6	82.5	24.7	79.5
e ^{nat}	83.2	90.2	88.2	87.7	86.5	84.3	91.4	90.7	85.9	79.8	88.1	87.1	87.7	25.2	81.1

Fe* = Fe²⁺ + Mn + Co + Cr + Ti + Fe³⁺;

e^{occ} = number of electrons at T(2) from assigned site-populations;

e^{nat} = number of electrons at T(2) from site-scattering refinement

* Mg

monly observed in unit formulae that the number of cations conventionally assigned to this site is significantly less than 4 apfu. In some cases, this will be due to the presence of undetermined Li. However, in general it indicates the presence of vacancies, and we know from previous arguments (Smith 1968) that occupancy of the *M*(4*A*) and *M*(4*B*) sites must be accompanied by vacancies at the locally associated *T*(2) sites.

Above we have given two "end-member" models for the occupancy-vacancy association of *M*(4*A*), *M*(4*B*) and *T*(2), the uncoupled model and the coupled model. Calculated vacancies are given Table 9, assuming the uncoupled model. Of course, these vacancies depend on the correct assignment of cations to *M*(4*A*) and *M*(4*B*) to account for the observed scattering; however, if there are major errors in any of the assignments, we should end up with an inconsistency in our scattering, chemical and stereochemical models. At this stage in the process of site-population assignments, it is not clear which occupancy-vacancy model is appropriate, and so we will retain both in our arguments.

Vacancies from stoichiometry

The results of the site-scattering refinements and the electron-microprobe analyses indicate the following sites to be fully occupied: *T*(1), *M*(1*A*), *M*(1*B*) and *M*(2), giving a total of 24 cations at these sites. The *M*(3*A*) and *M*(3*B*) sites have a combined rank of 4, and the *T*(2) site has a rank of 4. The resultant sum of sites corresponding to the formula unit with 48 [O, OH, F] is 32. This situation is complicated by the fact that the *M*(3*A*), *M*(3*B*) and *T*(2) sites are not fully occupied by cations, together with the occurrence of the *M*(4*A*) and *M*(4*B*) sites that also show only partial occupancy. As the *M*(3) site is on aggregate only (approximately) half occupied, and the vacancies at the *T*(2) site exceed the cations at *M*(4), the number of cations in the formula unit (CATSUM) generally ranges between 29.3 and 30.0 apfu; values for the staurolite crystals examined here are given in Table 6. These analytical values give us a check on our crystal-chemical assignment of vacancies; obviously we place more reliance on the compositions for which there are hydrogen determinations available.

TABLE 10. TRANSITION-METAL SITE-PREFERENCE IN STAULOLITE

Fe ²⁺	T(2) >> M(4)
Fe ³⁺	M(1), M(3) > M(2) > T(3)
Mn ²⁺	T(2)
Zn	T(2)
Co	T(2)
Ti ⁴⁺	M(2) >> M(1), M(3) ?

Assignment of cations

At this stage, we will assign all the remaining unassigned cations to the *T*(2) site and see how well they agree with the expected stoichiometry and refined scattering results; this is done in Table 9. The amount of Al at the *T*(1), *M*(1A), *M*(1B), *M*(2), *M*(3A) and *M*(3B) sites was calculated from the refined site-scattering (Table 5), and Mg was assigned to the *M* sites as discussed above; the Al assigned to these sites was subtracted from the total Al calculated from the microprobe analyses, and the remainder was assigned to the *T*(2) site. A similar procedure was followed with the other cations. To simplify this process, all transition metals (Fe²⁺, Fe³⁺, Mn, Co, Cr, Ti) are expressed as Fe^{*}; once we have assigned Fe^{*} site-populations, we can examine the behavior of the different minor transition-metal species. Above, we have shown that Li also occurs at the *T*(2) site in Li-rich staurolite crystals; this was so assigned for all crystals. This procedure produced slight negative occupancies for Al in three of the crystals. These negative amounts were within the uncertainty of the assignment procedure, and the Mg contents of the *M*(1,2,3) sites were adjusted slightly to remove these negative values; the amounts involved did not significantly affect the relationships shown in Figures 7, 11 and 12.

Summing the assigned contents of the *T*(2) site for all of the refined crystals gave cation (+ vacancy) sums between 3.88 and 4.00 apfu, compared to the ideal value of 4.00 apfu. We may ascribe these discrepancies to the presence of Fe^{*} atoms at the *M*(3) site, which we have not yet been able to assign, lacking any basis on which to do so. At this stage of the procedure, this situation has now changed. The deviations of the assigned *T*(2) cations (+ vacancy) from an ideal value of 4.0 are due to an excess of Fe^{*} and a deficiency of Al at *T*(2); this may be corrected by assigning to the *M*(3) site an amount of Fe^{*} equal to the difference between the *T*(2) sum and 4.0, and re-assigning twice that amount of Al to *T*(2). In this way, the scattering at each site is kept unchanged, whereas the scattering species at the *T*(2) site (including the assigned vacancy) now sum to the ideal value of 4.0 apfu; thus we have finally been able to assign the Fe^{*}

content of the *M*(3) site. The site-populations of Table 10 were assigned in this way. We note that for crystals S(17) to S(42), for which we assumed 3 H pfu, deviation from the assumption will adversely affect the *T*(2) site assignment, especially in the estimation of the Al content. This may be the origin of the high ^{*T*(2)}Al contents in a small number of crystals. Despite the very circuitous process of assignment for the *T*(2) site-populations, the number of electrons at the *T*(2) site calculated from the assigned populations corresponds reasonably well to the refined site-scattering values [R.M.S. deviation of 2.4 epfu with a mean value of ~84 epfu over the whole data set].

SITE ASSIGNMENTS FOR TRANSITION-METAL CATIONS

We have so far discussed the site populations of the transition metals in terms of the joint scattering species Fe^{*} = Fe²⁺ + Fe³⁺ + Mn + Co + Cr + Ti. We now need to assign specific *chemical* species to the various sites in the structure; we emphasize that this procedure is dependent on a wide variety of evidence in addition to the site-scattering refinement results discussed above.

Fe²⁺

Fe is dominantly in the divalent state in staurolite, and is also strongly ordered at the *T*(2) site; hence Fe²⁺ occurs at *T*(2). Fe also occurs at the *M*(4A) and *M*(4B) sites; both these sites are octahedrally coordinated, and as extensively discussed above, the observed mean bond-lengths indicate Fe²⁺ to occur at these sites. The combined site-scattering and observed mean bond-lengths at the *M*(1A), *M*(1B), *M*(3A) and *M*(3B) sites are incompatible with any significant Fe²⁺ occupancy of these sites. Thus Fe²⁺ occurs at the *T*(2), *M*(4A) and *M*(4B) sites (Table 10).

Fe³⁺

There have been a variety of proposals in the literature as to the location (and even existence) of Fe³⁺ in the staurolite structure; as the amounts of Fe³⁺ are very small, (i) it is very difficult to be sure (as distinct from guess) about the location of Fe³⁺, and (ii) we are not convinced by previous analytical and spectroscopic evidence that staurolite generally contains significant Fe³⁺. Caucia *et al.* (1994) have shown that combined oxidation – dehydroxylation occurs in staurolite (upon heating) *via* the process Fe²⁺ + OH → Fe³⁺ + O²⁻ + H↑. The resulting Fe³⁺ primarily occupies a *new* tetrahedrally coordinated site, the *T*(3) site (Table 1). Thus if small amounts of Fe³⁺ do occur in staurolite, they may either represent the original composition of the sample *or* the results of small amounts of postcrystallization oxidation–dehydroxylation.

As the $T(2)$ site accommodates small amounts of Al, it seems a reasonable argument that the $T(2)$ site could also accommodate small amount of Fe^{3+} . However, there is no *direct* evidence for this possibility, as Fe^{3+} can also occur at the tetrahedrally coordinated $T(3)$ site, and spectroscopic techniques (as distinct from scattering techniques) lack the spatial information to resolve this problem.

The total scattering due to transition metals at the $M(1A)$, $M(1B)$, $M(2)$, $M(3A)$ and $M(3B)$ sites is always in excess of the amount of (Ti+Cr), which also occur at these sites. Hence there must be small amounts (~0.1–0.2 apfu) of Fe^{3+} at these sites. If Ti^{4+} occurs primarily at $M(2)$, as suggested by Henderson *et al.* (1993), this would mean that $^{60}\text{Fe}^{3+}$ is strongly ordered at the $M(1A)$, $M(1B)$, $M(3A)$ and $M(3B)$ sites.

Mn^{2+}

Staurolite is not a characteristic mineral of highly oxidizing environments, and it is reasonable to assume that Mn is in the divalent state. Mn^{2+} is unlikely to substitute for Al at the $M(1A)$, $M(1B)$, $M(2)$, $M(3A)$ and $M(3B)$ sites, leaving the possible locations for Mn^{2+} as the $T(2)$, $M(4A)$ and $M(4B)$ sites. On the basis of size and charges arguments, one expects Mn^{2+} to behave in the same way as Fe^{2+} . As Fe^{2+} is strongly ordered at $T(2)$, it is reasonable to propose that Mn^{2+} shows the same behavior; as the Mn^{2+} contents of staurolite are low (<0.15 apfu), only the $T(2)$ site will show significant Mn^{2+} occupancy. Note that tetrahedral coordination of Mn^{2+} is uncommon but by no means unknown: ordered $^{41}\text{Mn}^{2+}$ occurs in willemite and in akatereite (Burns & Hawthorne 1993). These arguments are borne out by the results of Henderson *et al.* (1993), who showed *via* XAS that Mn in staurolite is tetrahedrally coordinated and (from the observed mean bond-length of 2.01 Å) in the divalent state.

Zn

The crystal structure results for natural Zn-rich staurolite (Hanisch 1966, this study) show Zn to be ordered at the $T(2)$ site. This behavior was also found for trace Zn in Fe-rich staurolite by Henderson *et al.* (1993), although they (in line with other previous suggestions in the literature) indicate that ^{66}Zn also could be present. We regard the latter suggestion as unlikely. Zn has a much stronger preference for tetrahedral coordination than Fe^{2+} , and there is always sufficient Fe^{2+} to account for the scattering at the $M(4A)$ and $M(4B)$ sites in the structure of any of the Zn-rich staurolite sample examined. A direct positive signal for ^{66}Zn needs to be recognized before this occupancy can be considered as confirmed.

Co^{2+}

From the occurrence and structure of lusakite (Bringhurst & Griffen 1986), Co^{2+} shows solid-solution with Fe^{2+} and occurs at the $T(2)$ site.

Ti^{4+}

Trivalent Ti is extremely rare in terrestrial environments (Waychunas 1987); Ti is assumed to be in the tetrahedral state in staurolite. As discussed above, the argument proposed for Ti^{4+} occupancy of $T(2)$ in staurolite is not convincing. As tetrahedrally coordinated Ti^{4+} is rare in minerals, it is a reasonable assumption that Ti^{4+} is octahedrally coordinated in staurolite. The $M(4A)$ and $M(4B)$ octahedra in staurolite are intrinsically quite large, and it seems unlikely that Ti^{4+} will occur at either of these sites. This leaves the $M(1A)$, $M(1B)$, $M(2)$, $M(3A)$ and $M(3B)$ sites as possible locations for titanium; however, as the amounts of Ti^{4+} involved are small (~0.10 apfu), our site-scattering refinements provided no direct evidence on this point, except to indicate that Ti^{4+} could occur at any or all of these sites. The XAS results of Henderson *et al.* (1993) support this argument, and further suggest that Ti^{4+} is strongly ordered at the $M(2)$ site.

CONCLUSIONS

1. Staurolite is monoclinic, $C2/m$, with β (observed) varying in the range 90.0–90.49°; the symmetry differences are reflected in the relative degree of order of the constituent cation species between the (pseudo-) equivalent A and B sites in the structure.
2. The β angle correlates linearly with the differential occupancy and size (mean bond-lengths) of the $M(3A)$ and $M(3B)$ octahedra; it is thus a measure of the degree of order in the structure. Other order–disorder pairs [*e.g.*, $M(4A)$ and $M(4B)$, possibly $T(2)$ site-splitting] also correlate with the β angle.
3. The mean bond-length of the $T(1)$ tetrahedron shows only very limited variation, reflecting the small variation in the Al content of the $T(1)$ site.
4. Site-scattering refinement shows small but significant amounts of transition metals at the octahedrally coordinated $M(1A)$, $M(1B)$, $M(2)$, $M(3A)$ and $M(3B)$ sites, which are dominantly occupied by Al.
5. Mean bond-length – composition relationships indicate significant occupancy of the $M(1)$, $M(2)$ and $M(3)$ sites by Mg; the slopes of these relationships allow quantitative assignment of Mg site-populations. In all except very Mg-rich staurolite crystals, approximately half of the Mg in the formula unit is in octahedral coordination.

6. There is a considerable range in $M(4)$ site-populations with varying bulk composition; expressed in terms of site scattering, the variation is 0–11.5 epfu. Several arguments indicate that the $M(4)$ sites are generally occupied by Fe^{2+} and vacancies, except for one very Mg-rich staurolite crystal ($\text{Mg} \approx 3.0$ apfu), in which $M(4)$ is occupied by Mg. In terms of atoms, the range of $M(4)$ site-populations is 0–0.43 Fe^{2+} apfu.

7. The variation in $M(4)$ occupancy shows a strong positive correlation with the H content.

8. There is variable total occupancy of the $M(3)$ sites, spanning the range 1.70–2.09 cations pfu. Low total occupancy correlates with increased H content.

9. The positional disorder of the $T(2)$ cations cannot be adequately resolved by conventional refinement of X-ray data. Even with data collected to maximum resolution ($2\theta_{\text{max}} = 135^\circ$), the model obtained is a function of the starting parameters of the refinement; this indicates convergence at local minima rather than at the global minimum. Consequently, although the data indicate cation disorder at $T(2)$, the quantitative results derived from normal procedures of refinement are not reliable.

10. Local order involving the $T(2)$ and $M(4)$ sites is a very important feature of the staurolite structure. Where $M(4A)$ or $M(4B)$ is occupied, the neighboring two $T(2)$ sites must be vacant (and *vice versa*). The stoichiometry of the staurolite crystals examined here indicates that a (locally) occupied $M(4)$ site is associated with vacant adjacent $M(4)$ sites. Thus the association of two $T(2)$ vacancies with an occupied $M(4)$ site is a long-range (as well as a short-range) feature of the structure, and allows quantitative assignment of vacancies to the $T(2)$ site from the assigned site-populations of the $M(4)$ site.

11. Li occupies the $T(2)$ site in Li-bearing staurolite.

12. The $T(2)$ site is occupied by Fe, Zn, Li, Co, \square , Mg and Al, and may be considered as chemically promiscuous.

ACKNOWLEDGEMENTS

We thank Luisa Ottolini, Piero Bottazzi and Marco Palenzona for their help with the ion-microprobe analysis, and all of the people who provided samples for this study: Christian Chopin, Barbara Dutrow, Ed Grew, Mike Holdaway, Bruno Lombardo, Annibale Mottana and Chris Ward. We thank Mike Henderson and coworkers for providing us with a copy of their paper on XAS of staurolite prior to publication. Barb Dutrow and Mike Holdaway suggested that FCH work on staurolite many years ago; they will pay for that!

We are indebted to the reviewers and to the editor who insisted that we clarify our fuzzy prose, and who very carefully checked the very involved arguments in this work; all errors are their fault. The CNR Centro di Studio per la Cristallografia e la Cristallografia, Pavia, provided an idyllic environment for this work. Financial support was provided by CNR–NATO, and the Natural Sciences and Engineering Research Council of Canada.

REFERENCES

- ALEXANDER, V.D. (1989): Iron distribution in staurolite at room and low temperatures. *Am. Mineral.* **74**, 610–619.
- BRINGHURST, K.N. & GRIFFEN, D.T. (1986): Staurolite – lusakite series. II. Crystal structure and optical properties of a cobaltoan staurolite. *Am. Mineral.* **71**, 1466–1472.
- BURNS, P.C. & HAWTHORNE, F.C. (1993): Edge-sharing Mn^{2+}O_4 tetrahedra in the structure of akatoreite, $\text{Mn}^{2+}_9\text{Al}_2\text{Si}_8\text{O}_{24}(\text{OH})_8$. *Can. Mineral.* **31**, 321–329.
- CAUCIA, F., CALLEGARI, A., OBERTI, R., UNGARETTI, L. & HAWTHORNE, F.C. (1994): Structural aspects of oxidation – dehydroxylation in staurolite. *Can. Mineral.* **32**, (in press).
- ČECH, F., POVONDRA, P. & VRANA, S. (1981): Cobaltoan staurolite from Zambia. *Bull. Minéral.* **104**, 526–529.
- DONNAY, J.D.H. & DONNAY, G. (1983): The staurolite story. *Tschermaks Mineral. Petrogr. Mitt.* **31**, 1–15.
- DUTROW, B.L. (1991): The effects of Al and vacancies on Li substitution in iron staurolite: a synthesis approach. *Am. Mineral.* **76**, 42–48.
- , HOLDAWAY, M.J. & HINTON, R.W. (1986): Lithium in staurolite: its petrologic significance. *Contrib. Mineral. Petrol.* **94**, 496–506.
- DYAR, M.D., PERRY, C.L., REBBERT, C.R., DUTROW, B.L., HOLDAWAY, M.J. & LANG, H.M. (1991): Mössbauer spectroscopy of synthetic and naturally occurring staurolites. *Am. Mineral.* **76**, 27–41.
- ENAMI, M. & ZANG, Q. (1989): Magnesian staurolite in garnet – corundum rocks and eclogite from the Donghai district, Jiangsu province, east China. *Am. Mineral.* **73**, 48–56.
- GREW, E.S. & SANDIFORD, S. (1984): A staurolite–talc assemblage in tourmaline – phlogopite – chlorite schist from northern Victoria Land, Antarctica, and its petrogenetic significance. *Contrib. Mineral. Petrol.* **87**, 337–350.
- GRIFFEN, D.T. (1981): Synthetic Fe/Zn staurolites and the ionic radius of $^{19}\text{Zn}^{2+}$. *Am. Mineral.* **66**, 932–937.
- , GOSNEY, T.C. & PHILLIPS, W.R. (1982): The chemical formula of natural staurolite. *Am. Mineral.* **67**, 292–297.

- & RIBBE, P.H. (1973): The crystal chemistry of staurolite. *Am. J. Sci.* **273-A**, 479-495.
- GROAT, L.A. & HAWTHORNE, F.C. (1989): The role of boron in the crystal structure of vesuvianite. *Geol. Assoc. Can. – Mineral. Assoc. Can., Program Abstr.* **14**, A81.
- , ——— & ERCIT, T.S. (1989): Boron \leftrightarrow hydrogen, the 'invisible' substitution in vesuvianite. *Geol. Assoc. Can. – Mineral. Assoc. Can., Program Abstr.* **14**, A97.
- , ——— & ——— (1992): The chemistry of vesuvianite. *Can. Mineral.* **30**, 19-48.
- HANISCH, K. (1966): Zur Kenntnis der Kristallstruktur von Staurolith. *Neues Jahrb. Mineral., Monatsh.*, 362-366.
- HAWTHORNE, F.C. (1990): Structural hierarchy in $M^{[6]T^{[4]}\phi_n}$ minerals. *Z. Kristallogr.* **192**, 1-52.
- , UNGARETTI, L., OBERTI, R., BOTTAZZI, P. & CZAMANSKE, G.K. (1993): Li: an important component in igneous alkali amphiboles. *Am. Mineral.* **78**, 733-745.
- HENDERSON, C.M.B., CHARNOCK, J.M., SMITH, J.V. & GREAVES, G.N. (1993): X-ray absorption spectroscopy of Fe, Mn, Zn and Ti structural environments in staurolite. *Am. Mineral.* **78**, 477-485.
- HOLDAWAY, M.J., DUTROW, B.L., BORTHWICK, J., SHORE, P., HARMON, R.S. & HINTON, R.W. (1986a): H content of staurolite as determined by H extraction line and ion microprobe. *Am. Mineral.* **71**, 1135-1141.
- , ——— & HINTON, R.W. (1988): Devonian and Carboniferous metamorphism in west-central Maine: the muscovite – almandine geobarometer and the staurolite problem revisited. *Am. Mineral.* **73**, 20-47.
- , ——— & SHORE, P. (1986b): A model for the crystal chemistry of staurolite. *Am. Mineral.* **71**, 1142-1159.
- & GOODGE, J.W. (1990): Rock pressure vs. fluid pressure as a controlling influence on mineral stability: an example from New Mexico. *Am. Mineral.* **75**, 1043-1058.
- HORNER, F. (1915): *Beitrage zur Kenntnis des Stauroliths*. Inaugural dissertation, Heidelberg, Germany.
- HURST, V.J., DONNAY, J.D.H. & DONNAY, G. (1956): Staurolite twinning. *Mineral. Mag.* **31**, 145-163.
- JUURINEN, A. (1956): Composition and properties of staurolite. *Ann. Acad. Sci. Fenn. Ser. A, III Geol.* **47**, 1-53.
- VON KNORRING, O., SAHAMA, T.G. & SIIVOLA, J. (1979): Zincian staurolite from Uganda. *Mineral. Mag.* **43**, 446.
- LEHMANN, M.S. & LARSEN, F.K. (1974): A method for location of the peaks in step-scan-measured Bragg reflexions. *Acta Crystallogr.* **A30**, 580-584.
- LONKER, S.W. (1983): The hydroxyl content of staurolite. *Contrib. Mineral. Petrol.* **84**, 36-42.
- NÁRAY-SZABÓ, I. (1929): The structure of staurolite. *Z. Kristallogr.* **71**, 103-116.
- & SASVÁRI, K. (1958): On the structure of staurolite $HF_2Al_9Si_4O_{24}$. *Acta Crystallogr.* **11**, 862-865.
- NORTH, A.C.T., PHILLIPS, D.C. & MATHEWS, F.S. (1968): A semi-empirical method of absorption correction. *Acta Crystallogr.* **A24**, 351-359.
- OTTOLINI, L., BOTTAZZI, P. & VANNUCCI, R. (1992): SIMS investigations of Li, Be, B in silicate minerals using CEF. *Goldschmidt Conf., Abstr. Program*, A-81.
- , ——— & ——— (1993): Quantification of Li, Be and B in silicates by secondary ion mass spectrometry using conventional energy filtering. *Anal. Chem.* (in press).
- PHILLIPS, L.V. & GRIFFEN, D.T. (1986): Staurolite – lusakite series. I. Synthetic Fe–Co staurolites. *Am. Mineral.* **71**, 1461-1465.
- PIGAGE, L.C. & GREENWOOD, H.J. (1982): Internally consistent estimates of pressure and temperature: the staurolite problem. *Am. J. Sci.* **282**, 943-969.
- POUCHOU, J.L. & PICHOR, F. (1984): A new model for quantitative analysis. I. Application to the analysis of homogeneous samples. *La recherche Aérop.* **5**, 47-65.
- & ——— (1985): 'PAP' $\phi(\rho Z)$ procedure for improved quantitative microanalysis. *Microbeam Anal.*, 104-106.
- RIBBE, P.H. (1982): Staurolite. In *Orthosilicates* (P.H. Ribbe, ed.). *Rev. Mineral.* **5**, 171-188.
- SCHREYER, W., HORROCKS, P.C. & ABRAHAM, K. (1984): High-magnesium staurolite in a sapphirine – garnet rock from the Limpopo Belt, southern Africa. *Contrib. Mineral. Petrol.* **86**, 200-207.
- & SEIFERT, F. (1969): High-pressure phases in the system $MgO - Al_2O_3 - SiO_2 - H_2O$. *Am. J. Sci.* **267-A**, 407-443.
- SHANNON, R.D. (1976): Revised effective ionic radii and systematic studies of interatomic distances in halides and chalcogenides. *Acta Crystallogr.* **A32**, 751-767.
- SKERL, A.C. & BANNISTER, F.A. (1934): Lusakite, a cobalt-bearing silicate from Northern Rhodesia. *Mineral. Mag.* **23**, 598-606.
- SMITH, J.V. (1968): The crystal structure of staurolite. *Am. Mineral.* **53**, 1139-1155.
- STÄHL, K., KVICK, Å. & SMITH, J.V. (1988): A neutron diffraction study of hydrogen positions at 13K, domain model, and chemical composition of staurolite. *J. Sol. State Chem.* **73**, 362-380.
- & LEGROS, J.-P. (1990): On the crystal structure of staurolite. The X-ray crystal structure of staurolite from the Pyrenées and Brittany. *Acta Crystallogr.* **B46**, 292-301.

- TAGAI, T. & JOSWIG, W. (1985): Untersuchungen der Kationenverteilung im Staurolith durch Neutronenbeugung bei 100 K. *Neues Jahrb. Mineral., Monatsh.*, 97-107.
- TAKÉUCHI, Y., AIKAWA, N. & YAMAMOTO, T. (1972): The hydrogen locations and chemical compositions of staurolite. *Z. Kristallogr.* **136**, 1-22.
- UNGARETTI, L. (1980): Recent developments in X-ray single crystal diffractometry applied to the crystal-chemical study of amphiboles. *God. Jugoslav. Kristalogr.* **15**, 29-65.
- , CALLEGARI, A. & CAUCIA, F. (1987): On the 'staurolite enigma'. *Terra Cognita* **7**, 384 (abstr.).
- , HAWTHORNE, F.C., CALLEGARI, A. & CAUCIA, F. (1988): Variazione cristallografiche indotte da riscaldamento su cristalli di staurolite. *Soc. Ital. Mineral. Petrol., Annual Meet. (Pavia)* (abstr.).
- , SMITH, D.C. & ROSSI, G. (1981): Crystal-chemistry by X-ray structure refinement and electron microprobe analysis of a series of sodic-calcic to alkali amphiboles from the Nybøo eclogite pod, Norway. *Bull. Minéral.* **104**, 400-412.
- WARD, C.M. (1984a): Magnesium staurolite and green chromian staurolite from Fiordland, New Zealand. *Am. Mineral.* **69**, 531-540.
- (1984b): Titanium and the color of staurolite. *Am. Mineral.* **69**, 541-545.
- WAYCHUNAS, G.A. (1987): Synchrotron radiation XANES spectroscopy of Ti in minerals: effects of Ti bonding distances, Ti valence, and site geometry on absorption edge structure. *Am. Mineral.* **72**, 89-101.

Received May 26, 1992, revised manuscript accepted December 4, 1992.